HAT 複合体構成因子 Brd1 の血液細胞における機能解析

2013

Yuta Mishima

Graduate School of Medical and Pharmaceutical Sciences

Chiba University

HAT 複合体構成因子 Brd1 の血液細胞における機能解析

先端生命科学専攻（分子細胞生物学研究室）　三嶋 雄太

【目的】真核細胞においてクロマチンは DNA とヒストンからなるヌクレオソームを最小単位として構成されている。近年、このヌクレオソームを構成するヒストン蛋白質の特定リジン残基におけるアセチル化によってヒストンの正電荷が中和され、ヌクレオソームの構造が弛緩することで、転写活性化に働くと考えられている。アセチル基の付加はヒストンアセチル基転移酵素 (histone acetyltransferase: HAT) により行われる。多くの場合、HAT は蛋白質複合体を形成し、その構成因子により HAT 活性や基質特異性等が制御される。そのため、HAT の構成因子の機能を明らかにできれば、HAT の活性制御や基質特異性の制御に関する新たな知見が得られると共に新しい創薬のターゲットとなる可能性も考えられる。本研究では、MYST (MOZ, Ybf2/Sas3, Sas2, and Tip60) ファミリーに属する HAT 複合体の構成因子である Brd1 (Bromodomain-containing protein 1) の個体レベルでの機能を明らかにすることを目的とした。

【背景】Brd1 はクロマチン制御因子に特徴的な機能ドメインを複数有する分子であり、Brpf2 とも呼ばれ、Brpf ファミリーに属する。同様のドメイン構造を有する Brpf1 は H3 HAT である MOZ/MORF と複合体を構成し、HAT 活性を増強する活性化因子として機能する事が報告されている。この事から Brd1 も HAT 複合体の構成要素として、ヒストン修飾を介した遺伝子発現制御に関与する可能性が考えられたが、その生理学的な機能は明らかにされていなかった。そこで、今回新たにノックアウトマウスを作製し、その機能解析を試みた。

【方法】個体レベルでの機能解析を行うため、Brd1 遺伝子欠損マウスを作製し、血液細胞をフローサイトメトリーで解析した。また、必要に応じて血液細胞をソーティングし、それらの細胞を用いた培養実験、タンパク結合実験、マイクロアレイ解析、Chromatin-immunoprecipitation on microarray (ChIP-Chip) 解析を行い Brd1 の機能を解析した。

【結果と考察】

① *Brd1*$^{-/-}$胎仔の胎生致死と形態異常

Brd1 の ATG 配列を含む exon2 を欠損させたノックアウトマウスを新規に作製したところ、*Brd1*$^{-/-}$マウスは胎齢（E）12.5-13.5 日において胎生致死である事が判明した。

E12.5 の *Brd1*$^{-/-}$マウスの形態を観察すると、ほとんどの個体で発達遅延（92/99 匹）、眼球の形成異常（74/122 匹）が観察され（図 1 A,B）、その他にも神経管の閉塞不全（30/135 匹）を示す個体も確認された。これらの所見から Brd1 は胎生期の発生過程において、様々な組織において重要な機能を有する事が考えられる。しかしながら、これらの異常は胎生致死の直接の原因とは考えにくく、主因は別にあるものと考えられた。

② *Brd1*$^{-/-}$胎仔肝における赤血球造血異常

胎生中期で起こる胎生致死の主因が貧血であることが多いことから、次に、この時期の造血組織である胎仔肝に注目し解析を進めた結果、胎仔肝の細胞数は野生型の 22%に減少していることが判明し（図 1 C,D）、胎仔肝の血液細胞の中には核が大きく未分化な赤芽球細胞が多く観察された（図 1 E,F）。赤血球分化の異常をより詳細に解析するため、トランスフェリンレセプターである CD71 と Ter119 を共染色してフローサイトメトリーによる解析を行った結果、未分化な赤芽球細胞（CD71^{+}Ter119^{-}細胞）が増加するとともに、

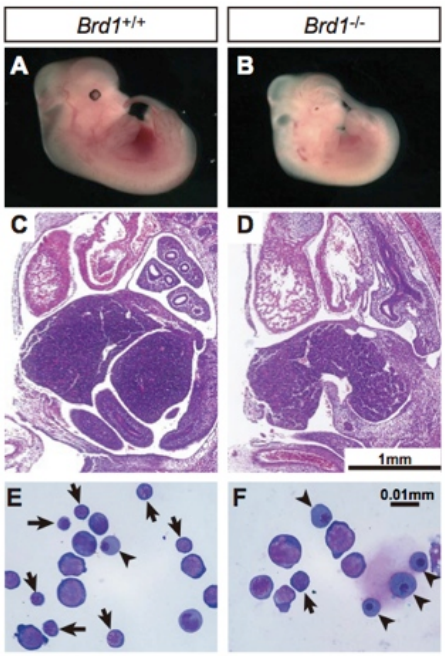

［図 1］胎齢 12.5 日の *Brd1*$^{-/-}$マウス
(A, B) 胎仔の顕微鏡像
(C, D) 胎仔肝の組織切片蔵
(E, F) 胎仔肝の血液細胞像
（矢印：成熟赤芽球細胞 矢尻：有核赤血球）

成熟した赤芽球（CD71^{+}Ter119^{+}細胞）が著しく減少することが確認された。Annexin V を用いた解析によりこれらの分画ではアポトーシスが亢進している事も明らかになった。この事から、Brd1 欠損による胎生致死は赤血球の分化異常による貧血が主因であると考えられた。

③ BRD1 は HBO1、ING4 と HAT 複合体を形成する

BRD1 と同じファミリー分子である BRPF1 は MOZ と HAT 複合体を形成する。そのため、BRD1 も MOZ と複合体を形成する可能性が考えられた。MOZ 欠損マウスも胎生致死であり、胎仔肝の造血異常を引き起こすことが報告されている。しかしながらその異常は主に造血幹細胞に認められ、Brd1 欠損マウスの赤血球分化異常とは異なる。そこで、BRD1 が形成する複合体を確認するため、Flag-BRD1 を発現するヒト白血病株 K562 細胞を用いて、BRD1 に結合するタンパク質を精製し、LC/MS/MS にて解析した。その結果、MYST ファミリーに属する HAT である HBO1 とその活性化因子 ING4 が同定された。Flag-BRD1 で精製した蛋白質の銀染色像を示す (図２A)。Flag-BRD1 が形成する複合体を免疫沈降し、HBO1、ING4 に対する抗体を用いてウェスタンブロッティングで確認を行ったところ、BRD1 は HBO1 と ING4 と複合体を形成することが確認された（図２B,C)。

次に、BRD1 と HBO1 の結合に関して、BRD1 のどの領域が重要なのかを確かめるため複数の断片化 BRD1 蛋白質（図２D）を用いて検証したところ、N 末端領域 (a.a. 1-198) が HBO1 との結合に必要である事が明らかとなった。

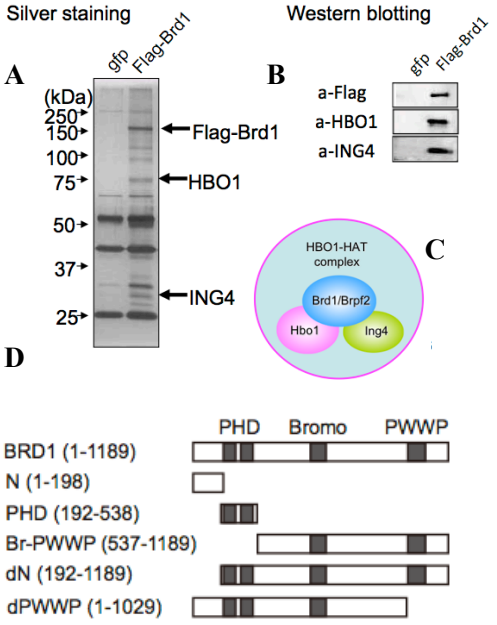

［図２］

(A) Flag-BRD1 で精製した結合蛋白質の銀染色像
(B) ウェスタンブロッティング
(C) BRD1-HBO1 HAT 複合体模式図
(D) 実験に使用した断片化 BRD1 蛋白質の構造

④ BRD1-HBO1 複合体は赤血球分化を促進する

ヒト白血病株 K562 は赤血球系へ分化誘導可能である細胞株である。この細胞の特性を利用して Brd1 欠損と赤血球分化異常との関連性を検証した。その結果 Brd1 の強制発現により K562 細胞の赤血球系への分化が促進される結果が得られた。しかしながら、HBO1 との結合に必要な N 末端領域 (a.a. 1-198) を除いた Brd1 の強制発現ではその効果が見られなかった。さらに、Hbo1 をノックダウンした K562 細胞ではヘモグロビン産生細胞が減少した事から、BRD1-HBO1 複合体が赤血球分化に機能を有している事が示された。

⑤ BRD1 と HBO1 は多くの遺伝子上で共局在している

次に、BRD1-HBO1 複合体が標的とする遺伝子を明らかにするため、K562 細胞を用いて ChIP-chip 解析を行った。その結果 BRD1 と HBO1 が多くの遺伝子上で共局在しており（図３A)、その局在ピークも転写開始点（TSS）を中心に非常に類似していることが判明した（図３B)。さらに、共局在している遺伝子リストの中には Gata1、Tal1 といった赤血球分化に重要な制御因子が含まれており、それらの遺伝子上において転写開始点を中心としたプロモーター領域に BRD1 と HBO1 が共局在していることが明らかになった（図３C)。

［図３］

(A) BRD1 と HBO1 の結合が検出された遺伝子の数
(B) TSS を中心とした全遺伝子結合シグナルの平均値
(C) Gata1 遺伝子上の BRD1 と HBO1 の局在シグナル

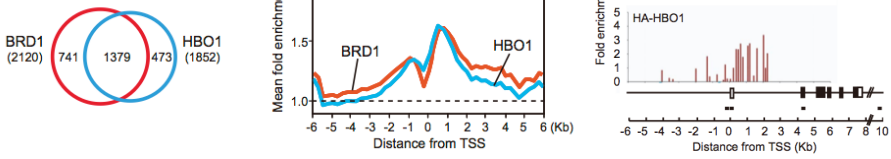

⑥ BRD1-HBO1 複合体はヒストン H3K14 のアセチル化に重要である

Brd1 複合体が実際に HAT 複合体として機能を持つかを検証するため、野生型と Brd1 欠損マウスからそれぞれ採取した赤芽球細胞 ($CD71^{+}Ter119^{-}$) を用いて、ヒストンのアセチル化を評価した。その結果、Brd1 欠損赤芽球では H3K14 のアセチル化が特に著しく減少している事が判明し、さらに、Hbo1 をノックダウンした赤芽球でも H3K14 のアセチル化レベルが減少することが確認された。その一方で、Brpf1 のパートナーである Moz 欠損マウスから採取した赤芽球細胞では H3K14 のアセチル化に変化は見られなかった。

また、H3K14 のアセチル化抗体を用いて行った ChIP 実験では、Brd1 欠損マウスの赤芽球において Gata1 をはじめとした赤血球分化に重要な遺伝子のプロモーター領域における H3K14 のアセチル化が減少していることが示された。これらの結果からも Brd1 が MOZ ではなく HBO1 と結合している事が示唆され、BRD1-HBO1 複合体が H3K14 のアセチル化に重要であると考えられた。

⑦ Brd1 は赤血球分化制御遺伝子群の転写制御に関与する

これまでの結果から、Brd1 の欠損により赤血球分化に重要な遺伝子群の転写抑制が予想されたため、定量 RT-PCR を用いて検証した。その結果、野生型と比較し Gata1 や Tal1 などの遺伝子発現が mRNA レベルで減少傾向にある事が示された。加えて、通常 Gata1 に負に制御されている Gata2 の mRNA レベルが逆に増加傾向にある事も示された。

このことから赤血球分化の重要な転写因子の一つである Gata1 に注目し、Brd1 を欠損した未分化な赤芽球前駆細胞（$c\text{-}Kit^{+}CD71^{-}$）に Gata1 を過剰発現させて培養実験を行ったところ、Brd1 を欠損した赤芽球の in vitro における増殖活性の回復が得られた。ただし、分化は十分な回復が得られなかった。

【結論】

以上の結果から、今回の研究によってクロマチン制御因子 Brd1 が Hbo1 と HAT 複合体を形成している事が明らとなった。また、Hbo1-Brd1 HAT 複合体によるヒストン H3K14 のアセチル化を介した Gata1 等の転写因子群の発現制御が、胎仔期の赤血球造血に重要な役割を果たすものと考えられた。（図４）

現在、成体での機能を検討するために Brd1 のコンディショナルノックアウトマウスを作製して解析を行っており、Brd1 が胸腺における免疫細胞の分化にも機能を有している事が明らかになっている。

これらの知見は、ヒストンのアセチル化を介した遺伝子制御機構の更なる解明に寄与するものと考えられる。

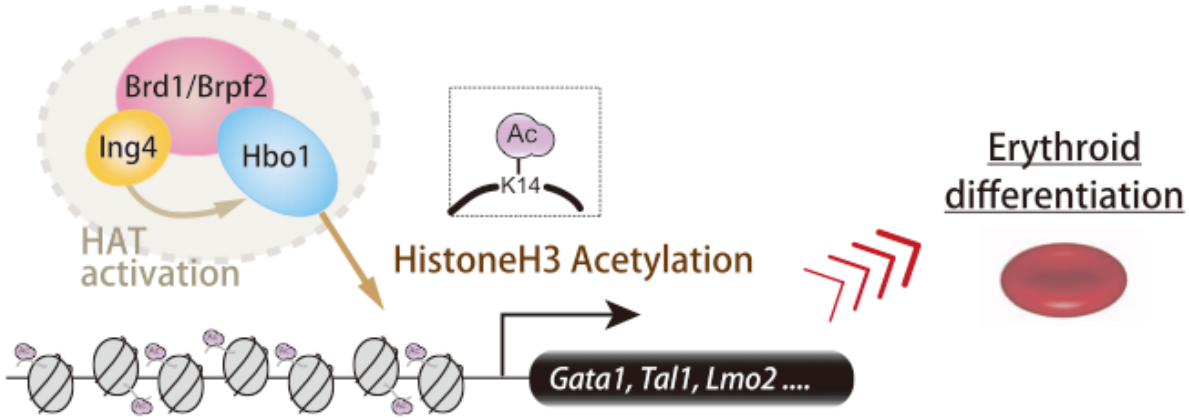

［図４］ Brd1-Hbo1 複合体が H3K14 のアセチル化によるクロマチンの構造変換を介した遺伝子発現制御機構に寄与し、胎仔期における Gata1 や Tal1、Lmo2 といった赤血球分化に重要な転写因子群の転写制御に機能していると考えられる。

Contents

HAT 複合体構成因子 Brd1 の血液細胞における機能解析 I

Contents 1

Abstract 3

Introduction 4

Materials and Methods 6
- Gene targeting of Brd1 6
- Viral production 6
- Purification of BRD1-containing protein complex 6
- Immunoprecipitation and extraction of histones 7
- ChIP-on-chip experiment 7
- cDNA cloning and expression vectors 8
- Antibodies 8
- Flow cytometric analysis 9
- HAT assay 10
- GST pull-down assay 10
- Histochemical and immunohistochemical analyses 11
- RT-PCR 11
- Primer sequences and probe numbers 12
- ChIP-on-chip experiment 13

Results 15
- *Brd1*$^{-/-}$ embryos die at mid-gestation because of anemia 15
- Brd1 is required for erythropoiesis in fetal liver 16
- BRD1 forms an active HAT complex with HBO1 and ING4 17
- The HBO1-BRD1 complex promotes erythroid differentiation 20
- Localization of the HBO1-BRD1 complex in the human genome 21
- Acetylation of H3K14 is specifically reduced in *Brd1*$^{-/-}$ mice 22

Discussion 25

Figures 29
Figure 1. Targeted disruption of the mouse *Brd1* gene. 29
Table 1. Analysis of *Brd1*-heterozygous intercross progenies. 30
Figure 2. Impaired hematopoiesis in *Brd1*$^{-/-}$ fetal liver. Appearance of wild-type 31
Figure 3. BRD1 forms a HAT complex with HBO1. 33
Figure 4. Overexpression of BRD1 induces erythroid differentiation in K562. 35
Figure 5. BRD1 and HBO1 coregulate erythroid genes. 37
Figure 6. The Hbo1-Brd1 complex is responsible for the bulk of H3K14 acetylation.....39
Figure 7. Insufficient transcription of erythroid regulator genes causes impaired erythropoiesis in *Brd1*$^{-/-}$ fetal livers. 41

Supplementary Figures.....43
Figure S1. Yolk sac and fetal liver hematopoiesis in *Brd1*$^{-/-}$ embryos. 43
Figure S2. Physical interaction among HBO1, BRD1, and ING4 in the complex. 44
Figure S3. Rescue of defective differentiatio of *Brd1*$^{-/-}$ erythroblasts by exogenous Brd1. 46
Figure S4. Stability of the BRD1 protein and the affinity of BRD1 for the MYST family HATs.....48
Figure S5. Effect of enforced expression of BRD1 on erythroid differentiation of K562 cells. 51
Figure S6. Levels of acetylation at H3 and H4 in *Brd1*$^{-/-}$ erythroblasts, MEFs, and brain. .52
Figure S7. Relationship between acetylation at H3K14 and BRD1-HBO1 binding. 54
Figure S8. Morphology of *Brd1*$^{-/-}$ CD71^{+}Ter119^{+} erythroblasts. 55

Acknowledgements 56

References 57

List of Publications 61

Examiners 62

Abstract

The histone acetyltransferases (HATs) of the MYST family include TIP60, HBO1, MOZ/MORF, and MOF and function in multisubunit protein complexes. Bromodomain-containing protein 1 (BRD1), also known as BRPF2, has been considered a subunit of the MOZ/MORF H3 HAT complex based on analogy with BRPF1 and BRPF3. However, its physiological function remains obscure. Here we show that BRD1 forms a novel HAT complex with HBO1 and regulates erythropoiesis. *Brd1*-deficient embryos showed severe anemia due to impaired fetal liver erythropoiesis. Biochemical analyses revealed that BRD1 bridges HBO1 and its activator protein, ING4. Genome-wide mapping in erythroblasts demonstrated that BRD1 and HBO1 largely co-localize in the genome and target key developmental regulator genes. Of note, levels of global acetylation of histone H3 at lysine 14 (H3K14) were profoundly decreased in Brd1-deficient erythroblasts and depletion of Hbo1 similarly affected H3K14 acetylation. Impaired erythropoiesis in the absence of Brd1 accompanied reduced expression of key erythroid regulator genes, including Gata1, and was partially restored by forced expression of Gata1. Our findings suggest that the Hbo1-Brd1 complex is the major H3K14 HAT required for transcriptional activation of erythroid developmental regulator genes.

Introduction

The histone acetyltransferases (HATs) of the MYST family, which include TIP60, HBO1, MOZ/MORF, and MOF, are highly conserved in eukaryotes and perform a significant proportion of all nuclear acetylation. They share a highly conserved MYST domain composed of an acetyl-CoA binding motif and a zinc finger and function in multisubunit protein complexes.[1,2] Among the MYST family members, HBO1 and MOZ/MORF form complexes of very similar composition: JADE family proteins bridge HBO1 with inhibitor of growth 4 and 5 (ING4/5) and Esa1-associated factor 6 ortholog (EAF6), whereas BRPF family proteins bridge MOZ/MORF with ING5 and EAF6, respectively.[1,3,4] The plant homology domain (PHD) fingers in JADE1/2/3, BRPF1/2/3, and ING4/5 interact with histones and are thought to define the substrate-specificity of the HBO1 and MOZ/MORF complexes.[1] HBO1 is considered responsible for the bulk of the acetylation of histone H4 at lysines 5, 8, and 12 (H4K5, K8, and K12), and the interaction between ING4 and histone H3 trimethylated at lysine 4 (H3K4me3) augments activity of HBO1 to acetylate histone H3.[5] Furthermore, the HBO1 complexes are enriched throughout the coding regions of genes, suggestive of a role in transcriptional elongation.[6] By contrast, MOZ and MORF are HATs specific for histone H3. Binding of Yng1, a yeast ortholog of the ING family, to H3K4me3 has been shown to promote Sas3 (yeast ortholog of MOZ) HAT activity at H3K14.[7] The mammalian MOZ complex also showed specificity for H3K14 acetylation in vitro.[3]

Moz-deficient mice have a severe defect in the maintenance of HSCs.[8,9] During zebrafish development, both *moz* and *brpf1* are required for maintenance of cranial *Hox* gene expression and proper determination of pharyngeal segmental identities.[10,11] Similar findings were reported from

analyses of *Moz*-deficient mice and medaka fish in which *brpf1* was mutated.[12] The genetic interaction between *Moz* and *Brpf1* supports that Brpf1 is the major bridging protein of the MOZ HAT complex. In contrast to Brpf1, however, distinctive functions of other BRPF family members have not been elucidated.

BRD1 (initially named BR140-LIKE; BRL) was originally cloned as a protein containing a cysteine-rich region related to that of AF10 and AF17, which are leukemic fusion partners of MLL.[13] BRD1 contains a bromodomain, 2 PHD zinc fingers, and a proline-tryptophan-tryptophan-proline (PWWP) domain, 3 types of modules characteristic of chromatin regulators. Recently, BRD1 was reported to belong to a small family of BRPF proteins that includes BRPF1, BRD1/BRPF2, and BRPF3.[1,3] BRD1 has been considered a subunit of the MOZ/MORF H3 HAT complex on the basis of analogy with BRPF1 and BRPF3.[3,4] However, no detailed analysis of BRD1 has been reported. In this study, we found that BRD1 forms a novel HAT complex with HBO1 and is responsible for the bulk of the acetylation of H3K14. We confirmed a drastic reduction in levels of acetylated H3K14 in *Brd1*-deficient mice and found that the Hbo1-Brd1 HAT complex is required for full transcriptional activation of the erythroid-specific regulator genes essential for terminal differentiation and survival of erythroblasts in fetal liver.

Materials and Methods

Gene targeting of Brd1

Brd1-deficient mice were generated by the use of R1 embryonic stem cells according to the conventional protocol. *Brd1*-deficient mice were backcrossed to the C57BL/6 background > 5 times. All experiments in which mice were used received approval from the Chiba University Administrative Panel for Animal Care.

Viral production

To prepare the retrovirus, pMC-ires-GFP was used as a vector.[14] The production and concentration of the recombinant retrovirus have been described previously.[15] To prepare the lentivirus, pCSII-EF1-MCS-IRESII-Venus and pCS-H1-shRNA-EF-1α-EGFP were used as vectors.[16] The viruses were produced as described previously. Target sequences were as follows; Sh-*mHbo1*#2; GAGGGAAGCAACATGATTA, Sh-*mHbo1*#3; GTGATGAGATTTATCGCAA, Sh-*hHBO1*#1; GGGATAAGCAGATAGAAGA, and Sh-*hHBO1*#3; CTCAAATACTGGAAGGGAA.

Purification of BRD1-containing protein complex

Protein purification, trypsin digestion, and liquid chromatography tandem mass spectrometry (LC/MS/MS) were performed as described previously.[17] In brief, K562 cells expressing Flag-Brd1 (2.5×10^8 cells) were suspended in 15 mL of lysis buffer (20 mM sodium phosphate, pH 7.0; 350 mM NaCl; 30 mM sodium pyrophosphate; 0.1% NP-40; 5 mM EDTA; 10 mM NaF; 0.1 mM Na_3VO_4; and 1 mM phenylmethylsulfonyl fluoride) containing protease inhibitors (cOmplete

mini; Roche) and sonicated for 20 minutes. The lysates were cleared by centrifugation and incubated with 100 μL of anti-FLAG M2 affinity gel (Sigma-Aldirch) with rotation at 4°C for 16 hours. The beads were extensively washed 6 times with 15 mL of lysis buffer. The complexes were eluted by incubating twice with 0.2 mg/mL of FLAG peptide in 300 μL of lysis buffer for 2.5 hours. This purification was repeated 10 times. Then, eluents were pooled and concentrated by the use of a filtration device (Vivaspin 10K-PES; Sartorius) and separated by 7.5%-15% SDS-PAGE.

Immunoprecipitation and extraction of histones

Transfected 293T cells were lysed in lysis buffer containing 250 mM NaCl and then immunoprecipitation was performed. Immunocomplexes were eluted with FLAG peptide as describe previously. Histone proteins were extracted following the method described previously.[18]

ChIP-on-chip experiment

ChIP-on-chip analyses of BRD1 and HBO1 binding were performed by use of the Human Promoter ChIP-on-chip Microarray Set (G4489A; Agilent Technologies). The assignment of IP regions and calculations were performed as described.[19] K562 cells were fixed with 1% formaldehyde in PBS for 10 minutes at room temperature and washed twice with PBS. Fixed cells swelled in the buffer (20 mM HEPES, pH 7.8; 1.5 mM $MgCl_2$; 10 mM KCl; 0.1% NP-40; and 1mM DTT) for 10 minutes on ice and nuclei were prepared by Dounce homogenizer. Nuclei were then lysed with RIPA (10 mM Tris, pH 8.0; 0.5% SDS; 140 mM NaCl; 1 mM EDTA; 1% TritonX-100; 0.1% SDS; 0.1% sodium deoxycholate; and a proteinase inhibitor cocktail [cOmplete mini]), and sonicated

for 30 minutes with a Bioruptor (Cosmobio Co Ltd). After centrifugation, the soluble chromatin fraction was precleared with a mixture of protein A and G-conjugated Dynabeads (Invitrogen) blocked with BSA and salmon sperm DNA. Three hundred micrograms of chromatin was immunoprecipitated overnight at 4°C with the use of 25 μL of antibody-conjugated Dynabeads. The immunoprecipitates were washed extensively and subjected to a quantitative PCR analysis with SYBR Premix Ex TaqTM II (Takara). For the ChIP of erythroblasts, the steps to prepare nuclei were omitted, and fixed cells were directly lysed by RIPA.

cDNA cloning and expression vectors

cDNA encoding a full-length Brd1 was cloned by PCR from the EML cell library, and cloned into the pcDNA3 vector. DNA fragments encoding full-length and truncated forms of Brd1 were amplified by PCR and subcloned into pcDNA3 containing sequences coding for Flag or HA. Expression vectors for HBO1, Tip60, MOZ, CBP, p300, and Brpf1 were described elsewhere. Details regarding expression vectors are available from the authors on request.

Antibodies

The following antibodies were used for Western blotting, immunostaining, immunoprecipitation and chromatin immunoprecipitation: anti-FLAG (clone M2; Sigma), anti-HA (clone 3F10; Roche), anti-HA (rabbit IgG, Santa Cruz), anti-MYC (9E10, Santa Cruz), anti-HBO1 (goat IgG, Santa Cruz), anti-ING4 (rabbit IgG, Proteintech group), anti-α-Tubulin (clone DM1A, Calbiochem), anti-acetyl-histone H3 (lys9), anti-acetyl-histone H3 (lys14), anti-histone H3 (rabbit IgG; Millipore), anti-acetyl-histone H4 (lys5) (cloneEP1000Y), anti-trimethyl-histone H3 (lys9) (rabbit IgG, abcam), anti-acetyl-histone H4

(lys8), anti-acetyl-histone H4 (lys12), anti-acetyl-histone H4 (lys16), anti-acetyl-histone H4, anti-histone H4, anti-trimethyl-histone H3 (lys27) (rabbit IgG; Millipore), anti-CD31/PECAM (G8.8; BD), and anti-active caspase3 (rabbit IgG, Chemicon). These antibodies were diluted appropriately according to the suppliers' recommendations. A polyclonal antibody against mouse Brd1 was generated by immunizing rabbits with recombinant N-terminal Brd1 (a.a. 1-456).

Flow cytometric analysis

Fetal liver cells were triturated with PBS containing 2% FBS and filtered through a nylon screen to obtain a single cell suspension. Yolk sacs were carefully separated and digested with 2 mg/ml of collagenase type I in the presence of 10% FBS at 37˚C for 1.5 h and triturated with PBS containing 2% FBS. Single cell suspensions of fetal liver and yolk sac were incubated with fluorochrome- and/or biotin-conjugated antibodies. Biotin-conjugated antibodies were detected with fluorochrome-conjugated Streptavidin. For Annexin V staining, fetal liver cells were suspended with 1xAnnexin binding buffer (BD), and stained with PE-conjugated CD71 and FITC-conjugated Ter119 antibodies, and APC-Annexin V (BD) following the manufacturer's protocol. For the staining of K562, cells were blocked with AB serum (sigma) for 20 min at room temperature and stained with antibodies. FACS analysis was performed with JSAN (Bay bioscience) or FACSCantoII (BD Biosciences), followed by an analysis with FlowJo software (Tree Star). Cell sorting was performed with a FACSAriaII (BD Biosciences) or JSAN using propidium iodide to exclude dead cells. The following antibodies were used for the flow cytometric analysis: CD45.2 (clone 104, FITC), CD71 (clone RI7217, PE), c-Kit (2B8, APC or PE-Cy7), Ter119

(clone TER-119, APC or Biotin), Dlk1 (clone 24-11, FITC), Glycophorin A (clone GA-R2, PE), and NGFR (clone C40-1457). Biotin-conjugated antibodies were visualized with Streptavidin-APC-Cy7.

HAT assay

K562 cells expressing Flag-Brd1 were suspended in 15 ml of lysis buffer [20 mM sodium phosphate pH 7.0, 350 mM NaCl, 30 mM sodium pyrophosphate, 0.1% NP-40, 5 mM EDTA, 10 mM NaF, 0.1 mM Na3VO4, and 1 mM phenylmethylsulfonyl fluoride (PMSF)] containing protease inhibitors (Complete mini, Roche) and sonicated for 20 min. The lysates were cleared by centrifugation and incubated with 100µl of anti-FLAG M2 affinity gel (sigma) with rotation at 4˚C for 16 h. The beads were extensively washed six times with 15 ml of lysis buffer. The immunoprecipitates, equivalent to $1x10^7$ cells, were mixed with 25 µl of HAT reaction mix containing 50 mM Tris pH 8.0, 10% glycerol, 0.1 mM EDTA, 1 mM dithiothreitol, 10 µM Acetyl CoA, and 0.1 mg/ml of recombinant histone H3 or H4. After 30 min at 30˚C, the reaction was stopped with the addition of SDS-sample buffer. The acetylation of histones was detected by Western blotting using specific antibodies.

GST pull-down assay

For GST pull-down assays, DNA fragments encoding the full-length HBO1 (GST-HBO1) and its MYST domain (GST-MYST), which encompasses 335 to 608 amino acids residues, were amplified by PCR and subcloned into the pGEX6p vector. GST fusion proteins were expressed in BL21 (DE3) cells. For the GST pull-down assay, HA-tagged Brd1 or dN was translated in vitro using a TNT reticulocyte lysate transcription/translation system (Promega) and

mixed with GST-fusion proteins. The reaction was carried out in lysis buffer containing 150 mM NaCl at 4˚C for 2 h and the beads were washed four times with the same buffer.

Histochemical and immunohistochemical analyses

The embryos were fixed in formalin and embedded in paraffin. The 10 μm sections were subjected to hematoxylin and eosin staining. For immunohistochemical analyses, fetal livers dissected from 12.5 dpc embryos were fixed with 4% PFA, cryoprotected in 30% sucrose, frozen in OCT materials, and sectioned at 12 μm.

RT-PCR

Total RNA was extracted using Trizol reagent according to the manufacturer's instructions (Invitrogen). cDNA was synthesized from total RNA using ThermoScript RT-PCR System (Invitrogen). Quantitative RT-PCR was carried out by using TaqMan Universal PCR Master Mix (Applied Biosystems), Universal ProbeLibrary (Roche), and the Applied Biosystems 7300 Fast Real-Time PCR system (Applied Biosystems).

Primer sequences and probe numbers

Brd1 5’-AATGGTGCTCCCCTGTTG-3’, 5’-TGGCAGCTTTCATCTCTTCAT-3’,
probe #95

Hbo1 5’-GAGTCACCCGCTCCTCAG-3’, 5’-TGGAGTTCGAGGTGGTGAC-3’,
probe #66

Gata1 5’-TCCCAGTCCTTTCTTCTCTCC-3’, 5’-CACACACTCTCTGGCCTCAC-3’,
probe #66

Gata2 5’-GCTTCACCCCTAAGCAGAGA-3’, 5’-TGGCACCACAGTTGACACA-3’,
probe #15

Tal1 5’-GCTCGCCTCACTAGGCAGT-3’, 5’-ACCCGGTTGTTGTTGGTG-3’,
probe #60

Cbfa2t3 5’-GTGGTCCATGGTCTGTCTCTT-3’, 5’-AAGCCATTGGGTGTAGATGG-3’,
probe #66

Stat5a 5’-CAACATGTACCCACCCAACC-3’, 5’-CTGGCAACATCCATGCTCT-3’,
probe #85

Stat5b 5’-TTTATCACAGTGGATCGAAAGC-3’, 5’-GGGTGGCCTTAATGTTCTCC-3’,
probe #95

Bcl-xl 5’-CCTTGGATCCAGGAGAACG-3’, 5’-CAGGAACCAGCGGTTGAA-3’,
probe #66

Hprt1 5’-TCCTCCTCAGACCGCTTTT-3’, 5’-CCTGGTTCATCATCGCTAATC-3’,
probe #95.

ChIP-on-chip experiment

Primer sequences:

human GATA1

Promoter 5’-GCTTAGCCTGGGTCATCAAG-3’ and

5’-GGATGTGGCTGTACCCATTT-3’

TSS 5’-CTTGTCTTTGCCCCACTCTC-3’ and

5’-TACTGAGCAGGCAGGGAGTT-3’

Exon2 5’-TGTCCTCCACACCAGAATCA-3’ and

5’-TCCCTGTAGTAGGCCAGTGC-3’;

Down 5’-TAAGCCCTGACCTCAGCCTA-3’ and

5’-CCAGTACCAGTCCGTGTCCT-3’;

human TAL1

promoter 5’-CTTTCCCCCTTTGTTGGTCT-3’ and

5’-AGGGGGCTTGGAGAGAGATA-3’

Exon1 5’-GAGGGGTTGTTGTTGCTGTT-3’ and

5’-AGGTGTTTGGAGCCTTTCCT-3’

Exon4 5’-AGGGCCTGGTTGAAGAAGAT-3’ and

5’-CACAGGCTTAGGAAGGCAAG-3’;

human Albumin

promoter 5’-TGGCAGCCAATGAAATACAA-3’ and

5’-AACACACCCCTGGAATAAGC-3’

mouse Gata1

5’-ACCTGCAAAATGGGTACAGC-3’ and

5’-AGGCTATGTGTGGGTTGGAC-3’

mouse Gata2

5’-GAGTTTGGGGAGTCAGTTGG-3’ and

5’-GACGTGCACCTTCTGGGTAT-3’

mouse Stat5a

5’-GATCAGGAACTCGGAATGGA-3’ and

5’-TGGCTGCCTACTCGAATACC-3’

mouse Tal1

5’-CCAGTTTTAGAGCGGTCAGG-3’ and

5’-ACCAACCCTCCCTTCTTCAT-3’

mouse Albumin

5’-GCAAACATACGCAAGGGATT-3’ and

5’-ACCTCGCATTTCATTGGTTC-3’.

Results

Brd1$^{-/-}$ embryos die at mid-gestation because of anemia

To clarify the physiologic function of Brd1, we generated *Brd1*-deficient mice in which exon 2 containing the first ATG of the *Brd1* gene was deleted (Figure 1A). Northern blot analysis detected no *Brd1* mRNA in *Brd1*$^{-/-}$ embryos (data not shown). The *Brd1*$^{-/-}$ embryos were recovered at nearly the expected Mendelian ratio at 12.5 days postcoitum (dpc) but most had died by 15.5 dpc (Table 1). *Brd1*$^{-/-}$ embryos showed growth retardation (92 of 99 embryos at 12.5 dpc), failure to fuse the neural tube (30 of 135 embryos at 8.5-12.5 dpc), and abnormal lenses with disoriented optic cups (74 of 122 embryos at 10.5-12.5 dpc; Figure 1B and Table 1). These results indicated Brd1 as having pivotal roles in embryonic development in multiple tissues and organs, but none of them was considered to be the cause of death.

We then analyzed hematopoiesis in the absence of Brd1. Numbers of total yolk sac cells and Ter119^{+} erythroblasts were rather increased in *Brd1*$^{-/-}$ yolk sac compared with those in wild-type yolk sac (Figure 1C-D). This trend was more apparent at later stages. At 12.5 dpc, erythropoiesis was still active in *Brd1*$^{-/-}$yolk sac, whereas erythropoiesis tended to decline in wild-type yolk sac (supplemental Figure 1A). Together, our findings suggest that primitive erythropoiesis in the *Brd1*$^{-/-}$ yolk sac was not affected but rather enhanced. Nevertheless, *Brd1*$^{-/-}$ embryos at 12.5 dpc were pale and the fetal liver, in which fetal hematopoiesis mainly occurs, was significantly smaller than that of littermate controls (Figure 2A-D). Cytologic analysis revealed that *Brd1*$^{-/-}$ fetal livers had profoundly fewer erythroblasts beyond the proerythroblast stage than did wild-type fetal livers (Figure 2E-F).

Brd1 is required for erythropoiesis in fetal liver

Among the phenotypes associated with *Brd1* deficiency, we focused on anemia, which is a major causative defect for lethality at this stage of development. Flow cytometric analysis of fetal livers at 12.5 dpc revealed a 2-fold reduction in the $Ter119^+$ erythroid cell fraction and a 2-fold increase in the c-Kit^+ hematopoietic progenitor fraction (Figure 2G). Because the total number of $Brd1^{-/-}$ fetal liver cells was decreased to 22% of the control, the absolute number of $Ter119^+$ erythroid cells was decreased by 91% in $Brd1^{-/-}$ fetal livers compared with wild-type fetal livers, whereas that of c-Kit^+ hematopoietic progenitors was not profoundly changed (Figure 2H). The number of $Dlk1^+$ hepatoblasts was reduced to 57% of the control, but the differentiation of hepatoblasts into hepatocytes and cholangiocytes was grossly normal in the$Brd1^{-/-}$ fetal liver (Figure 2G-H; and data not shown). These results indicated that the fetal liver hypoplasia in $Brd1^{-/-}$ embryos was mainly caused by a reduction in numbers of erythroid lineage cells.

Detailed flow cytometric analyses revealed a significant increase in the $CD71^+Ter119^-$ fraction and a drastic reduction in the $CD71^+Ter119^+$ and $CD71^-Ter119^+$ fractions in $Brd1^{-/-}$ fetal livers compared with wild-type fetal livers (Figure 2I-J). The $CD45^-$c-$Kit^+CD71^+Ter119^-$ CFU-erythroid fraction was also more prevalent in $Brd1^{-/-}$ fetal livers (Figure 2J top). These results indicate a differentiation block of $Brd1^{-/-}$ fetal liver erythroblasts at the transition from $CD71^+Ter119^-$ to $CD71^+Ter119^+$ stage. Nonetheless, absolute numbers of cells in each fraction, particularly the $CD71^+Ter119^+$ and $CD71^-Ter119^+$ fractions, were significantly decreased (Figure 2J bottom). To further elucidate the mechanism by which *Brd1* deficiency causes defective erythropoiesis, we examined the apoptosis of erythroblasts. Apoptotic cells with an active caspase-3

were readily detected in *Brd1*$^{-/-}$ fetal livers (supplemental Figure 1B). The number of annexin V^{+}/7-aminoactinomycin D^{-} apoptotic cells was also significantly elevated in *Brd1*$^{-/-}$ fetal livers; cell death was even further exacerbated in the CD71^{+}Ter119^{+} and CD71^{-}Ter119^{+} fractions (Figure 2K). Thus, loss of Brd1 in fetal liver erythroblasts causes massive apoptosis and maturation delay, leading to severe anemia. These findings suggested that severe anemia combined with other physiologic defects accounts for the death of *Brd1*$^{-/-}$ embryos.

BRD1 forms an active HAT complex with HBO1 and ING4

Analogous to BRPF1, BRD1/BRPF2 has been proposed to form a H3 HAT complex with MOZ.[3,4] Similar to *Brd1*$^{-/-}$ mice, *Moz*$^{-/-}$ mice die in the embryonic stage and show impaired fetal liver hematopoiesis. However, the hematopoietic defect in *Moz*$^{-/-}$ fetal livers is observed mainly in HSCs.[8,9] To address this discrepancy, we purified BRD1-containing protein complexes by Flag epitope-specific immune-affinity purification from K562 human leukemic cells expressing Flag-BRD1 and analyzed them by LC/MS/MS (Figure 3A). The LC/MS/MS analysis identified several proteins as putative components of the BRD1 complex. Among these proteins, we focused on ING4 and HBO1 because HBO1 and ING4 were reproducibly and substoichiometrically copurified with Flag-BRD1 in our repeated purifications. Immunoblotting of the purified fraction confirmed the presence of HBO1 and ING4 in the complex (Figure 3B). HBO1 and MOZ have been demonstrated to form similar protein complexes with ING4/5, JADE1/2/3, and hEAF6 and ING5, BRPF1/2/3, and hEAF6, respectively, in HeLa cells.[1,2] JADE and BRPF family proteins function as a bridging protein between HBO1 and ING4/5 and MOZ and ING5, respectively.

To determine the physical interaction among HBO1, BRD1, and ING4 in the complex, we transfected 293T cells with different combinations of *BRD1*, *HBO1*, and *ING4*. HBO1 and ING4 were coimmunoprecipitated only in the presence of BRD1, whereas BRD1 was coimmunoprecipitated with HBO1 or ING4 in the absence of ING4 and HBO1, respectively (supplemental Figure 2A-C). These results indicate that BRD1 functions as a scaffold to link HBO1 with ING4 and form a ternary complex. To confirm the formation of a complex between the endogenous Brd1 and Hbo1 proteins, we immunoprecipitated Brd1 with an anti-Brd1 antibody from both wild-type and *Brd1*$^{-/-}$ whole embryos at 12.5 dpc. Of note, Hbo1 was detected in the immunoprecipitates from wild-type but not *Brd1*$^{-/-}$ embryos (supplemental Figure 2E).

The Brd1 mutants containing the N-terminal 198 amino acids (N and dPWWP) interacted with HBO1, whereas fragments lacking the N-terminal 192 amino acids did not (PHD, Br-PWWP, and dN; (Figure 3C-D). These results indicate that the N-terminal 198 amino acids of BRD1 are necessary and sufficient for physical interaction with HBO1. Conversely, the BRD1-interacting domain was localized to the MYST domain of HBO1 (supplemental Figure 2D). We then tested whether the complementation of *Brd1*$^{-/-}$ progenitors with exogenous *Brd1* can rescue their compromised erythroid differentiation in vitro. We purified c-Kit^{+}CD71^{-} hematopoietic progenitors from 12.5 dpc fetal livers. The cells were retrovirally transduced with the wild-type *Brd1* or dN mutant and then cultured for 3 days in the presence of erythropoietin (EPO) to induce erythroid differentiation (supplemental Figure 3). As expected, wild-type *Brd1* but not dN mutant considerably canceled the differentiation block of *Brd1*$^{-/-}$ erythroblasts at the transition from CD71^{+}Ter119^{-} to CD71^{+}Ter119^{+} stage. These results further support the formation of a complex

between BRD1 and HBO1 through the N terminus of Brd1.

We also noted that coexpression of HBO1 increases the protein level of BRD1 (Figure 3D; see inputs of BRD1, N, and dPWWP) in 293T cells. The treatment of the cells with MG132, a proteasome inhibitor, also increased the BRD1 protein level, strongly suggesting that HBO1 stabilizes the BRD1 protein by inhibiting the proteasome-dependent protein degradation pathway (supplemental Figure 4A). Similar levels of protein stabilization were observed when HBO1 was coexpressed with BRD1 deletions retaining an HBO1-binding capacity, but not dN, which lacked the HBO1-binding domain (supplemental Figure 4A), indicating that the N-terminal 198 amino acids are required not only for BRD1-HBO1 interaction but also for stability of the BRD1 protein. These findings further support the formation of a complex between BRD1 and HBO1.

We then examined the interaction of BRD1 with various HATs. Coimmunoprecipitation assays demonstrated that BRD1 binds mainly to HBO1 and TIP60, moderately to MOZ, and not at all to CBP and p300 (Figure 3E). In contrast, BRPF1 preferred MOZ and bound moderately to HBO1 (supplemental Figure 4B). The difference in affinity for HATs between BRD1 and BRPF1 was evident when they were forced to compete with each other to form complexes. This experiment clearly showed that BRD1 and BRPF1 prefer to bind with HBO1 and MOZ, respectively (supplemental Figure 4C).

The HBO1 HAT complex is reportedly responsible for the bulk of the acetylation of H4K5, K8, and K12 and also acetylates histone H3.[3,5,20] The BRD1 complex from K562 cells efficiently acetylated the recombinant histone H4 at K5, K8, and K12, but not K16, and moderately acetylated the recombinant histone H3 at K9 and 14 (Figure 3F). These findings implied that BRD1 and HBO1 form a novel HAT complex that differs in composition from known HAT complexes.

The HBO1-BRD1 complex promotes erythroid differentiation

K562 human leukemic cells, which we used for purification of the BRD1 complex, have a potential to differentiate along the erythroid lineage. We found that overexpression of BRD1 promotes hemoglobinization of K562 cells (clone BRD1c2, Figure 4A). Enhanced hemoglobin production was confirmed by benzidine staining in BRD1c2 (Figure 4B, benzidine-positive cells, control cells 5.3% ± 0.4% vs BRD1c2 18.4% ± 0.3%) and in a series of other clones (supplemental Figure 5A-B, control cells 5.7% ± 2.3% vs Flag-BRD1 25.6% ± 6.7%). Expression of glycophorin A, an erythroid lineage marker antigen, on the cell surface, was also significantly increased in the BRD1-overexpressing clones (supplemental Figure 5C-D, control cells 29.0% ± 0.3% vs Flag-BRD1 72.0% ± 0.2%). These results indicated that BRD1 induces erythroid differentiation of K562 cells.

To understand the mechanism of the BRD1-mediated erythroid differentiation, we examined the impact of BRD1 deletions on erythroid differentiation of K562 cells. The capacity of BRD1 to induce erythroid differentiation was profoundly affected by deletion of the N-terminus, which mediates interaction with HBO1 (dN mutant; Figure 4C), although the dN mutant was expressed and localized to the nucleus (data not shown). In contrast, the C-terminal deletion mutant (dPWWP) still had a significant effect (Figure 4C). Both BRD1 and dPWWP significantly reduced cell growth probably as a consequence of erythroid differentiation (Figure 4D). These results indicate that the HBO1-binding domain is indispensable for BRD1 to induce erythroid differentiation. We also tested the effect of BRPF1, which mostly binds to MOZ, and found that BRPF1 does not induce erythroid differentiation (Figure 4E), implying that the HBO1-BRD1 complex has a distinct function from the

MOZ-BRPF1 complex in erythroid cells. We then examined whether HBO1 has a significant impact on erythroid differentiation by knocking down its expression. We transduced K562 cells with lentiviruses expressing shRNA against the human HBO1 (sh*HBO1*#1 and #3) and a scrambled control shRNA sequence. The percentages of benzidine^{+} cells were significantly reduced by *HBO1* knockdown even in uninduced K562 cells (Figure 4F).

Localization of the HBO1-BRD1 complex in the human genome

To identify the direct target genes of the HBO1-BRD1 complex, we conducted a ChIP-on-chip analysis in K562 cells coexpressing 3xFlag-BRD1 and HA-HBO1, and we identified 2120 and 1852 genes bound by BRD1 and HBO1, respectively (full data are listed in supplemental ChIP-chip dataset). Of these, 1379 genes were co-occupied by BRD1 and HBO1, indicating that BRD1 and HBO1 coregulate a significant portion of their target genes in erythroid cells (Figure 5A). The peaks of BRD1 and HBO1 signals coincided around −1.0 kb and 1.0 kb from the transcription start site (TSS; Figure 5B). Then, we examined the relationship between the degree of HBO1-BRD1 binding and transcription status by using published data on expression profiles of K562 cells examined with microarrays.[21] The HBO1- or BRD1-occupied genes tended to be expressed in K562 cells (Figure 5C), indicating that the HBO1-BRD1 complex generally activates transcription of their target genes. The functional annotation of the set of genes bound by both BRD1 and HBO1 was performed on the basis of gene ontology and showed significant enrichment for genes that fell into the categories "transcriptional coactivator activity" ($P < .015$), "transcriptional factor activity" ($P < .018$), and "structural constituent of the ribosome" ($P < .042$).

Of note, targets included erythroid master regulator

genes, *GATA1*, *TAL1/SCL*, and *LMO2*, and other regulator genes such as *CBFA2T3/ETO2*, *STAT5A*, and *STAT5B*. The binding of HBO1 and BRD1 was detected throughout the coding regions of genes with peaks around TSS (Figure 5D-E).

Acetylation of H3K14 is specifically reduced in *Brd1*$^{-/-}$ mice

To test for a function of Brd1 as a histone modifier, we compared histone acetylation in CD71^{+}Ter119^{-} and CD71^{+}Ter119^{+} erythroblasts between *Brd1*$^{-/-}$ and *Moz*$^{-/-}$ fetal livers. Of note, the level of global acetylation of H3K14 was profoundly decreased in *Brd1*$^{-/-}$ erythroblasts by 70%-80% and that of H3K9 was also moderately decreased, whereas those of H4K5, K8, and K12 were not significantly changed (Figure 6A and supplemental Figure 6A). In contrast, the levels of global acetylation of H3K9 and H3K14 did not change in *Moz*$^{-/-}$ erythroblasts (Figure 6A). Similar results were obtained with *Brd1*$^{-/-}$ and *Moz*$^{-/-}$ mouse embryonic fibroblasts (MEFs) and *Brd1*$^{-/-}$ brain (supplemental Figure 6B-C). In contrast, the levels of representative repressive histone modifications, H3K9me3 and H3K27me3, were not largely changed in erythroblasts and MEFs (supplemental Figure 6D-E). ChIP assays confirmed global reductions in levels of H3K14 acetylation in the promoter regions of both erythroid (*Gata1*, *Stat5a*, and *Tal1*) and nonerythroid (Albumin; Alb) genes (Figure 6B). Furthermore, the ChIP-on-chip analysis in K562 revealed that H3K14 were highly acetylated at the TSS/promoter region of 46.9% of the genes bound by both BRD1 and HBO1, including *GATA1*, *TAL1/SCL*, *CBFA2T3/ETO2*, and *STAT5A* (supplemental Figure 7). These findings support our biochemical findings that BRD1 forms a HAT complex with HBO1 but not MOZ and imply that this complex is responsible for the bulk of H3K14 acetylation.

We then tested whether the depletion of HBO1 in erythroblasts recapitulates the defective erythropoiesis of *Brd1*$^{-/-}$ fetal livers. We purified c-Kit^{+} CD71^{-} hematopoietic progenitors from 12.5 dpc fetal livers. The cells were transduced with *Hbo1* knockdown lentiviruses and then cultured for 3 days in the presence of EPO to induce erythroid differentiation (Figure 6C). Of note, the frequency of CD71^{+}Ter119^{+} erythroblasts in the green fluorescent protein positive (GFP^{+}) knockdown cells was significantly reduced with sh-*Hbo1*#2 and #3 (Figure 6C). Quantitative RT-PCR analysis of the erythroblasts revealed that sh-*Hbo1*#3 knocked down *Hbo1* more efficiently than #2 (#2, 44.7%, and #3, 19.1% of the control). Correspondingly, the block in erythroid differentiation was more pronounced by knockdown with #3. These results indicate that *Hbo1*knockdown perturbs differentiation of fetal liver erythroid progenitors in a fashion similar to the absence of *Brd1*. Importantly, levels of H3K14 acetylation were severely reduced in *Hbo1*-knockdown erythroblasts and H3K9 acetylation was also significantly reduced (Figure 6D). In addition, levels of H4K5 and K8 acetylation were moderately reduced in *Hbo1*-knockdown erythroblasts (Figure 6D).

We then compared the expression levels of erythroid transcription factors in wild-type and *Brd1*$^{-/-}$ erythroblasts by quantitative RT-PCR. As expected, mRNA expression of *Gata1*, *Scl/Tal1*, and *Lmo2*,[22–26] erythroid master regulator genes that appeared to be the direct targets of the HBO1-BRD1 complex in K562 cells, was mildly decreased in *Brd1*$^{-/-}$ erythroblasts (Figure 7A). Furthermore, expression of *Gata2*, the gene negatively regulated by Gata1,[27,28] was up-regulated in *Brd1*$^{-/-}$ CD71^{+}Ter119^{+} erythroblasts. These expression patterns implied that the impaired functions of erythroid transcription factors, particularly Gata1, is responsible for the defective erythropoiesis in *Brd1*$^{-/-}$ fetal livers. To

test this hypothesis, we transduced c-Kit^{+}CD71^{-} hematopoietic progenitors from 12.5 dpc fetal livers with *Gata1* and cultured them for 3 days in the presence of EPO to induce erythroid differentiation (Figure 7B). Notably, forced expression of *Gata1* efficiently restored the proliferative capacity and survival of *Brd1*$^{-/-}$ erythroblasts (Figure 7B). Of note, however, it only partially canceled the differentiation block at the CD71^{+}Ter119^{-} to CD71^{+}Ter119^{+} transition (Figure 7B). Furthermore, the morphologic analyses of the purified CD71^{+}Ter119^{+} erythroblasts revealed no obvious defects in morphologic maturation of *Brd1*$^{-/-}$ CD71^{+}Ter119^{+} erythroblasts even in the absence of exogenous *Gata1* (supplemental Figure 8). These results suggest that dysregulated expression of *Gata1* mainly accounts for impaired proliferation and survival of *Brd1*$^{-/-}$ erythroblasts.

Discussion

In this study, we identified a novel HAT complex consisting of HBO1, BRD1, and ING4. BRD1 was believed to be involved in the MOZ HAT complex on the basis of analogy to BRPF1[3,4] but appeared to prefer to form a complex with HBO1. The finding that HBO1 stabilized the BRD1 protein further supported the physiologic significance of this complex. The levels of H3K14 acetylation were profoundly reduced in all cells and organs examined in *Brd1*$^{-/-}$ mice and *Hbo1*-knockdown erythroblasts. Thus, this complex is responsible for the bulk of H3K14 acetylation in general. Very recently, loss of Hbo1 in mice was reported to lead to a significant reduction of H3K14 acetylation, but not to affect acetylation at other histone residues.[29] These observations correspond well to ours and support our notion that BRD1 functions in the HBO1 HAT complex. However, residual H3K14 acetylation was evident in *Brd1*$^{-/-}$ cells, suggesting the existence of other H3K14 HATs. These might include the Moz-Brpf1 complex, which reportedly acetylates H3K9 and K14,[7,30] although the levels of H3 acetylation were not affected in *Moz*$^{-/-}$ erythroblasts or MEFs in this study. In addition, another Hbo1 HAT complex, which involves Jade family proteins,[3,20] might also contribute to the acetylation of H3K14, although its capacity to acetylate H3K14 has not been tested. This notion is supported by the finding that *Hbo1* knockdown affected levels of H3K14 acetylation more severely than the depletion of Brd1 in erythroblasts.

HBO1 and MOZ/MORF MYST HAT complexes target chromatin via multiple PHD finger-based interactions with histone H3 tails.[5] The PHD finger of ING4 recognizes and binds to H3K4me3.[5–7] JADE and BRPF family proteins share 2 highly conserved PHD fingers that function in chromatin binding. Given their similar composition, the HBO1 and MOZ/MORF HAT complexes likely

regulate acetylation of H3K14. Nonetheless, the absence of Brd1 had little or no impact on the acetylation of H3K9 and H4 (K5, K8, and K12) whereas *Hbo1* knockdown considerably affected the acetylation of H3K9 and H3K14 and marginally reduced levels of acetylated H4K5 and K8. *Jade1L* knockdown reportedly decreased bulk histone H4 acetylation in 293T cells.[20] These findings highlight differences in specificity among these HAT complexes.

HBO1 was originally cloned as a binding partner of origin recognition complex 1, a subunit of the DNA replication initiation complex, and interacts with MCM2, a component of the MCM helicase complex.[31,32] According to accumulating evidence,[3,33,34] HBO1 has a crucial role in regulation of the prereplicative complex assembly and initiation of DNA replication. In contrast, recent findings also unveiled its role in transcriptional regulation, sometimes in concert with transcription factors. Two closely related HBO1 complexes with different ING proteins (either ING4 or ING5) have been characterized and MCM proteins were specifically copurified with the ING5-HBO1 complex, suggesting that the ING5 complex functions in DNA replication whereas the ING4 complex is involved in transcriptional regulation. Actually, *ING5* knockdown in 293T cells completely blocks cell-cycle progression through the S phase.[3] Thus, composition, ie, the recruitment of either ING4 or ING5, may hold the key to context-dependent function of HBO1. BRD1 forms a complex with HBO1 and ING4 and loss of Brd1 impaired the maturation and/or survival of erythroblasts, but not their proliferation, indicating that the transcription-related function of Hbo1 is mainly affected in *Brd1*-deficient erythroid cells. However, Kueh et al[29] observed no defects in DNA replication or cell proliferation in *Hbo1* mutant embryos, MEFs, or immortalized fibroblasts. Role of Hbo1 in DNA replication

might require careful reevaluation using *Hbo1*-deficient cells.

It is widely recognized that the N-terminal tail of histone proteins is acetylated in the promoter region of actively transcribed genes and acetyl-lysine residues are recognized by bromodomain-containing factors in general. Although the role of acetylation at H3K9 and K14 is not well understood compared with that of histone methylation, H4K8 and K12 acetylation is reportedly followed by H3K9 and K14 acetylation at the IFNβ promoter after a viral infection.[35] In this cascade, H4K8 acetylation mediates recruitment of the SWI/SNF complex via the bromodomain-containing BRG1 subunit, whereas the acetylation of H3K9 and K14 is critical to the recruitment of TFIID via a tandem bromodomain factor, TAFII250. This coordinated recruitment of transcriptional complexes participates in the transcriptional induction of the *IFN*-β gene. However, the BAF complex is reported to be anchored to promoters by acetylated H3K14 though the BAF57 subunit, which contains a bromodomain.[36] Therefore, the BRD1-HBO1 complex might be involved in the recruitment of transcriptional complexes to promoters via H3K14 acetylation and exert activity in transcriptional initiation. However, the binding of BRD1 and HBO1 was detected throughout the coding regions of genes, although the peaks were detected around TSS. Therefore, we cannot eliminate a role for the HBO1 HAT complex in transcriptional elongation as proposed by Saksouk et al.[6] The recognition of H3K36me3, an epigenetic mark for transcriptional elongation, by the PWWP domain of Brpf1 supports this notion.[37]

Among the study of various developmental defects observed in *Brd1*$^{-/-}$ embryos, detailed analyses of erythropoiesis highlighted a crucial role for the HBO1-BRD1 complex in transcriptional activation of developmental regulator genes. The process of erythropoiesis is well orchestrated at the molecular level

by a complex network of transcription factors, including *Gata1*, *Gata2*, and*Scl/Tal1*.[24,26] A genome-wide ChIP-chip analysis clearly demonstrated that the HBO1-BRD1 complex targets genes involved in "transcriptional regulation," including these key erythroid regulator genes. Among them, the transcription factor gene *Gata1* is required for terminal erythroid maturation and functions as an activator or repressor depending on context. *Gata1*-deficient embryos are severely anemic and their fetal liver erythroblasts have a differentiation block at the $CD71^{+}Ter119^{-}$ stage and undergo massive apoptosis.[22,24,26] Although the reduction in *Gata1* expression was mild in $Brd1^{-/-}$ erythroblasts, the expression of *Gata2*, an erythroid regulator gene negatively regulated by Gata1, was mildly but significantly derepressed, and impaired $Brd1^{-/-}$ erythropoiesis was partially restored by the expression of *Gata1*. Given that the Hbo1-Brd1 complex regulates global H3K14 acetylation in erythroblasts, the defective erythropoiesis could not be attributed solely to *Gata1*. The failure of exogenous *Gata1* to release differentiation block of $Brd1^{-/-}$ erythroblasts supports this notion. Nevertheless, all these findings provide the first evidence of a crucial role for the HBO1-BRD1-ING4 complex and H3K14 acetylation in the transcriptional activation of key developmental regulator genes required for development and differentiation.

The MYST family HATs are involved in various aspects of tumorigenesis as transcriptional regulators.[1] Overexpression of HBO1 has also been reported in various human cancers.[38] Intriguingly, BRD1 fused to PAX5 (PAX5-BRD1) has recently been implicated in acute lymphoblastic leukemia.[39] This fusion protein is thought to ectopically activate transcription of PAX5 target genes by recruiting HBO1. Thus, our findings also provide a molecular basis to understanding the complex functions of HBO1 in cancer.

Figures

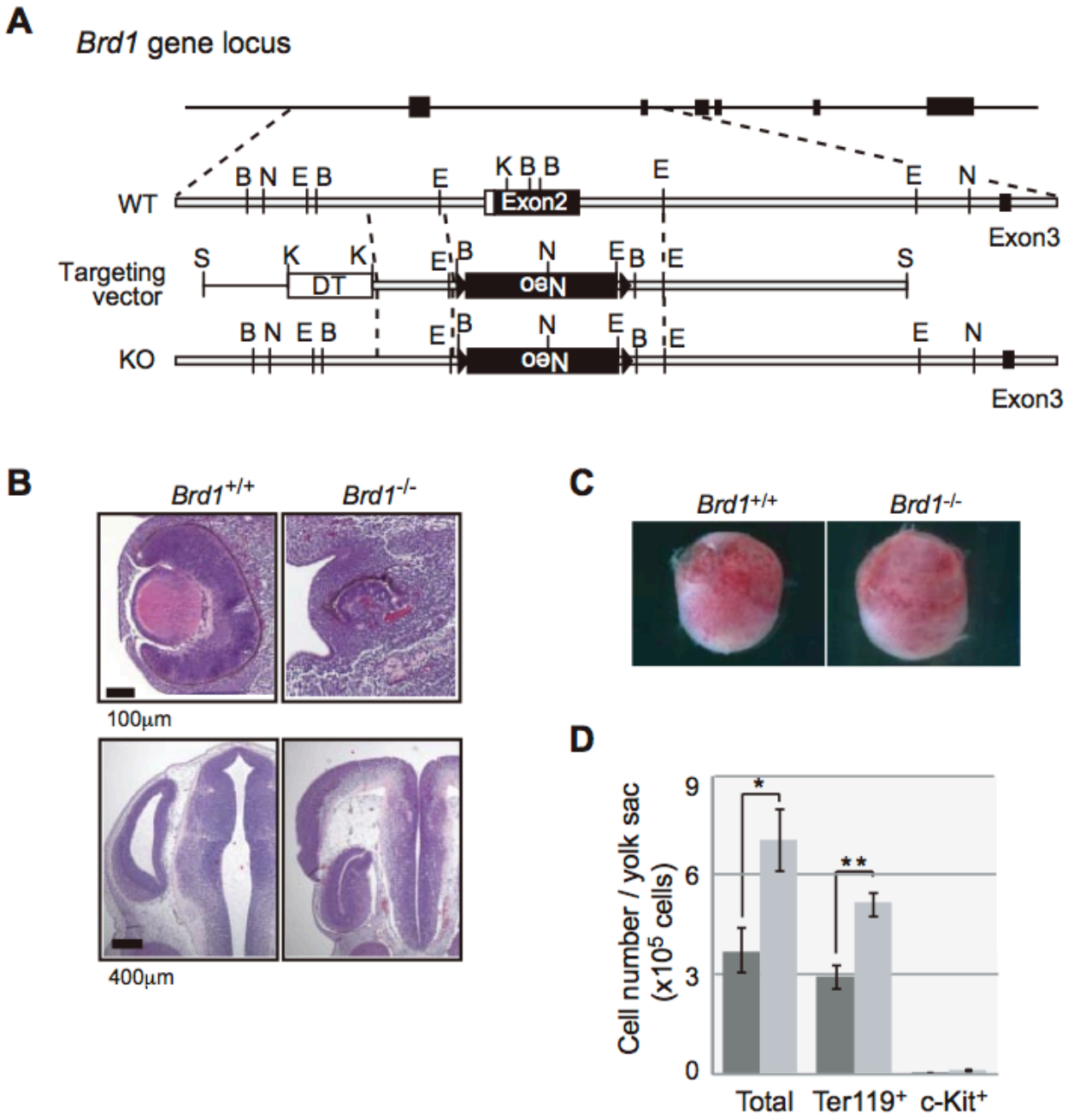

Figure 1. Targeted disruption of the mouse *Brd1* gene.

(A) Strategy for making a knockout allele for *Brd1* by homologous recombination in ES cells. B, BamHI; N, NcoI; E, EcoRI; K, KpnI; S, SalI. (B) Developmental defects in *Brd1*$^{-/-}$ embryos. Abnormal lenses with disoriented optic cups (top) and neural tube disclosure (bottom) in *Brd1*$^{-/-}$ embryos at 12.5 dpc. Sections were stained with hematoxylin and eosin. (C) Appearance of

wild-type (*Brd1*$^{+/+}$, left) and *Brd1*$^{-/-}$ (right) yolk sac at 10.5 dpc. (D) Absolute numbers of total cells, c-Kit^{+} hematopoietic progenitors, and Ter119^{+} erythroid cells in 10.5 dpc yolk sac from wild-type (left bar, n = 5) and Brd1$^{-/-}$ (right bar, n = 3) embryos. The results are shown as the mean ± SE *P < .05, **P < .005.

Table 1. Analysis of Brd1-heterozygous intercross progenies.

Stage, dpc	*Brd1*$^{+/+}$	*Brd1*$^{+/-}$	*Brd1*$^{-/-}$	ND	Total progenies
8.5-9.5	5	20	13 (1)*†	3	41
10.5-11.5	24	49	23 (2)‡§¶	5	101
12.5	117	238 (2)	99 (4)#‖**	44	498
13.5	10	15	2††	1	28
14.5-15.5	4	22	1	6	23
16.5-18.5	3	4	0	13	20
Weaning	17	23	0	0	40

Numbers in parentheses indicate dead embryos.
dpc indicates days postcoitum; and ND, not determined.
*Six embryos showed growth retardation.
†Four embryos showed failure to fuse the neural tube.
‡Twenty-one embryos showed growth retardation.
§Two embryos showed failure to fuse the neural tube.
¶Three embryos showed abnormal eye development.
#Ninety-two embryos showed growth retardation.
‖Twenty-four embryos showed failure to fuse the neural tube.
**Seventy-one embryos showed abnormal eye development.
††One embryo showed abnormal eye development.

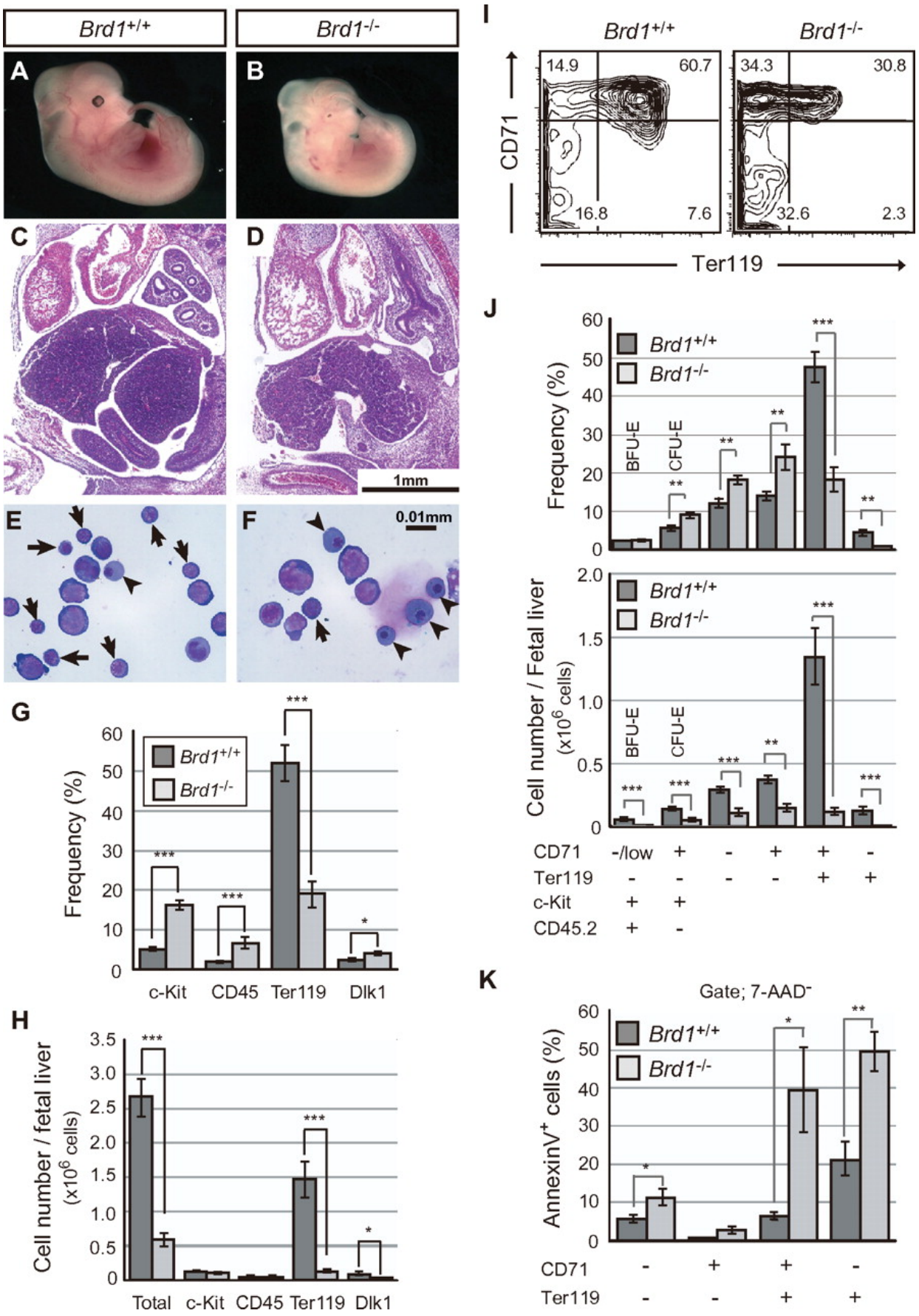

Figure 2. Impaired hematopoiesis in *Brd1*$^{-/-}$ fetal liver. Appearance of wild-type

(A) and *Brd1*$^{-/-}$ (B) embryos at 12.5 dpc. H&E-stained transverse sections of

12.5 dpc wild-type (C) and *Brd1*$^{-/-}$ (D) embryos. Morphology of 12.5 dpc fetal liver hematopoietic cells from wild-type (E) and *Brd1*$^{-/-}$ (F) embryos stained with May-Grüenwald-Giemsa solutions. Arrows and arrowheads indicate mature erythroblasts and nucleated erythrocytes, respectively. Frequency (G) and absolute cell numbers (H) of c-Kit^{+} hematopoietic progenitors, CD45^{+} hematopoietic cells, Ter119^{+} erythroid cells, and Dlk1^{+} hepatoblasts in 12.5 dpc fetal livers from wild-type and Brd1$^{-/-}$ embryos. The results are shown as the mean ± SE ($n \geq 4$). *$P < .05$, ***$P < .0005$. (I) Flow cytometric profiles of erythroid differentiation defined by CD71 and Ter119 expression in representative fetal livers at 12.5 dpc. The percentage of each fraction is indicated. (J) Frequency (top) and absolute cell numbers (bottom) of BFU-E, CFU-erythroid, CD71^{-}Ter119^{-} cells, CD71^{+}Ter119^{-} erythroblasts, CD71^{+}Ter119^{+} erythroblasts, and CD71^{-}Ter119^{+} erythroblasts in 12.5 dpc fetal livers from wild-type and Brd1$^{-/-}$ embryos. The results are shown as the mean ± SE ($n \geq 8$). **$P < .005$, ***$P < .0005$. (K) Massive apoptosis of Brd1$^{-/-}$ erythroblasts. The percentage of annexin V^{+}/7-aminoactinomycin D^{-} (7-AAD^{-}) apoptotic cells in each fraction defined by CD71 and Ter119 is shown as the mean ± SE ($n \geq 4$). *$P < .05$, **$P < .005$.

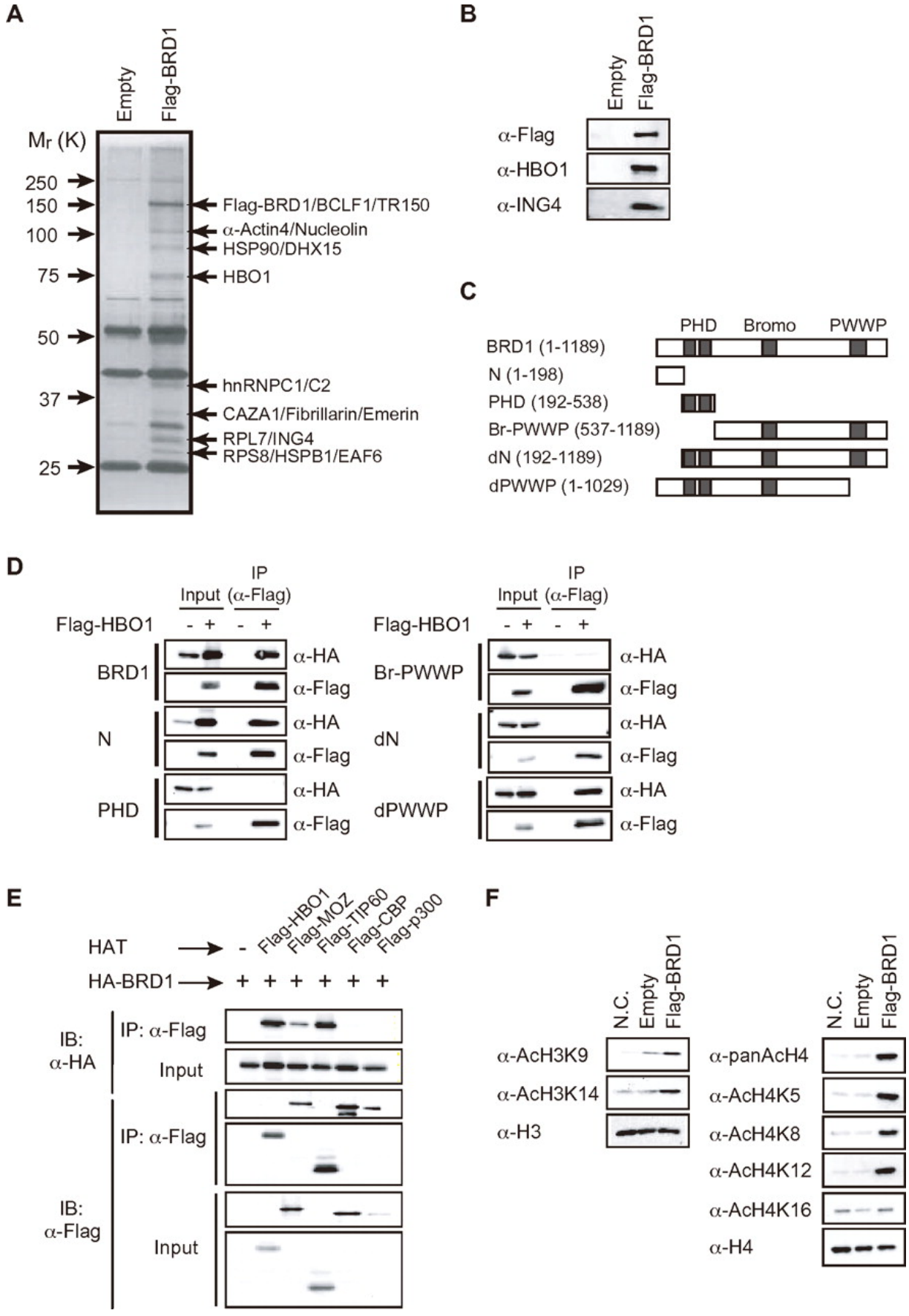

Figure 3. BRD1 forms a HAT complex with HBO1.

(A) Purification of the BRD1 complex. Flag-tagged BRD1 protein was partially

purified from lysates of K562/Flag-BRD1 cells using an anti-Flag antibody. (B) Western blot analysis of the purified BRD1 complex in panel A by the use of indicated antibodies. (C) Schematic representation of BRD1 and its deletion mutants. Three major domains are indicated. (D) Localization of the binding site in BRD1 for HBO1. 293T cells were transfected with HA-tagged BRD1 mutants with and without Flag-tagged HBO1. Proteins in the lysates of the transfectants were immunoprecipitated with the anti-FLAG antibody and eluted with an excess of Flag peptide. The eluents were analyzed by Western blotting by the use of anti-Flag or HA antibodies. (E) Affinity of BRD1 for the MYST family HATs (HBO1, MOZ, and Tip60) and CBP/p300. 293T cells were transfected with HA-tagged Brd1 together with indicated Flag-tagged HATs. Proteins in the lysates of the transfectants were immunoprecipitated with the anti-FLAG antibody. The immunoprecipitates were analyzed by Western blotting with anti-Flag and HA antibodies. (F) HAT activity of the BRD1 complex. The BRD1 complex was partially purified from lysates of K562/empty vector (Empty) and K562/Flag-BRD1 cells by the use of the anti-Flag antibody and HAT activity on recombinant histones H3 and H4 was evaluated. As a negative control (N.C.), the recombinant histones H3 and H4 were similarly treated without HAT complexes.

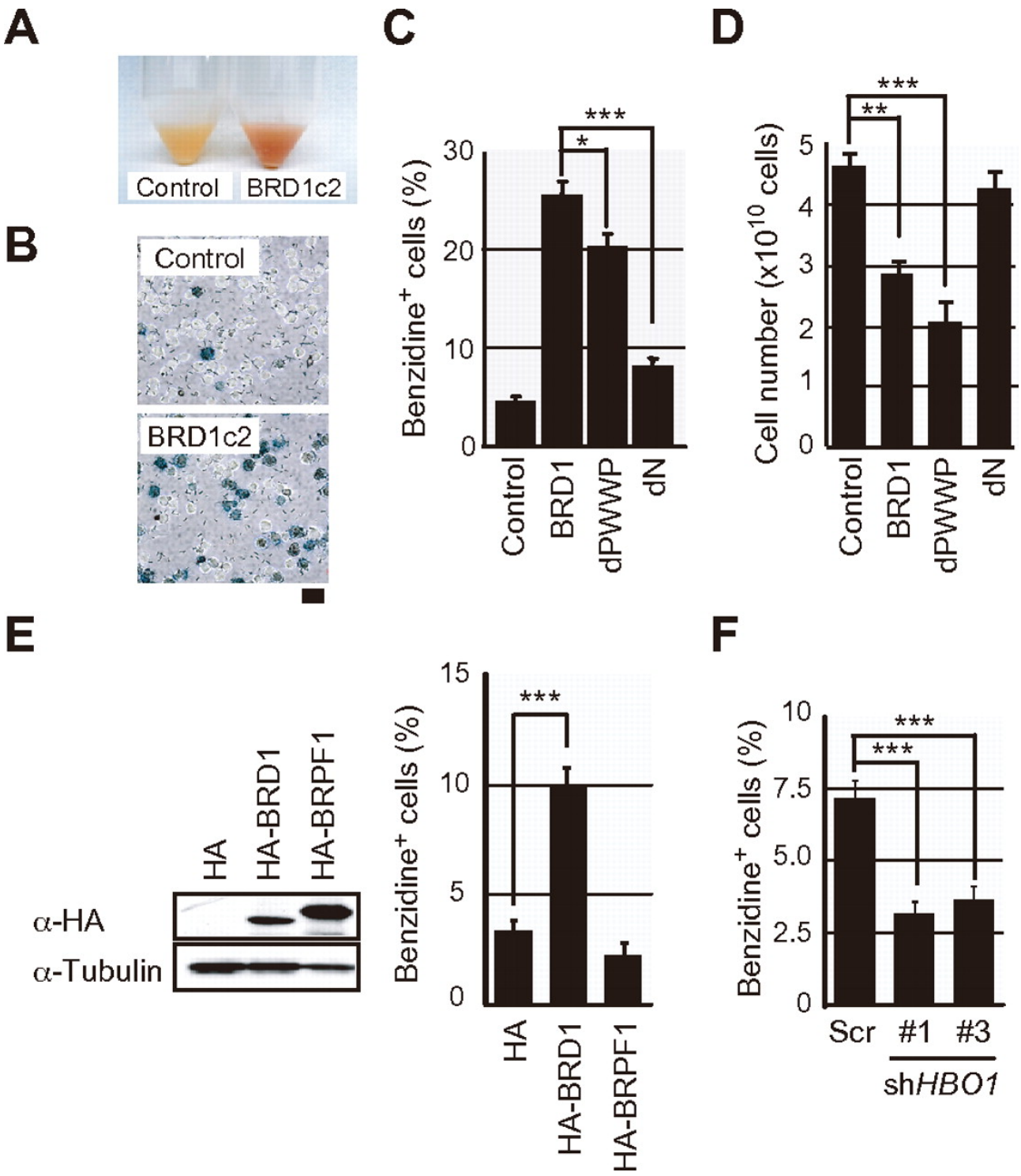

Figure 4. Overexpression of BRD1 induces erythroid differentiation in K562.

(A) Appearance of parental K562 cells (Control) and the Flag-BRD1-expressing clone (BRD1c2) used for purification of the BRD1 complex. (B) Benzidine staining of parental K562 cells (Control) and Brd1c2. The bar indicates 20 μm (C) Benzidine staining of K562 cells expressing BRD1 mutants. K562 cells were transduced with an empty vector (Control) or retroviruses expressing full-length

BRD1 (BRD1), dPWWP, or dN. Transduced cells were sorted with the use of GFP as a marker antigen and expanded for benzidine staining. Bars represent mean ± SE (n = 12). (D) Growth of K562 cells expressing BRD1 or the BRD1 mutant in (C). The results are shown as the mean ± SE for triplicate cultures. (E) Overexpression of BRPF1 in K562 cells. K562 cells were transduced with a HA-BRPF1 retrovirus, and BRPF1 expression was detected by Western blotting by use of the anti-HA antibody (left). Effects of BRPF1 on erythroid differentiation of K562 cells were evaluated by benzidine staining. The data are shown as the mean ± SE for triplicate cultures. (F) Knockdown of HBO1 with the use of shRNA. K562 cells were infected with lentiviruses expressing shRNAs against HBO1 and analyzed as to the basal status of hemoglobinization by benzidine staining. The results are shown as the mean ± SE for triplicate cultures. *P < .05, **P < .005, ***P < .0005.

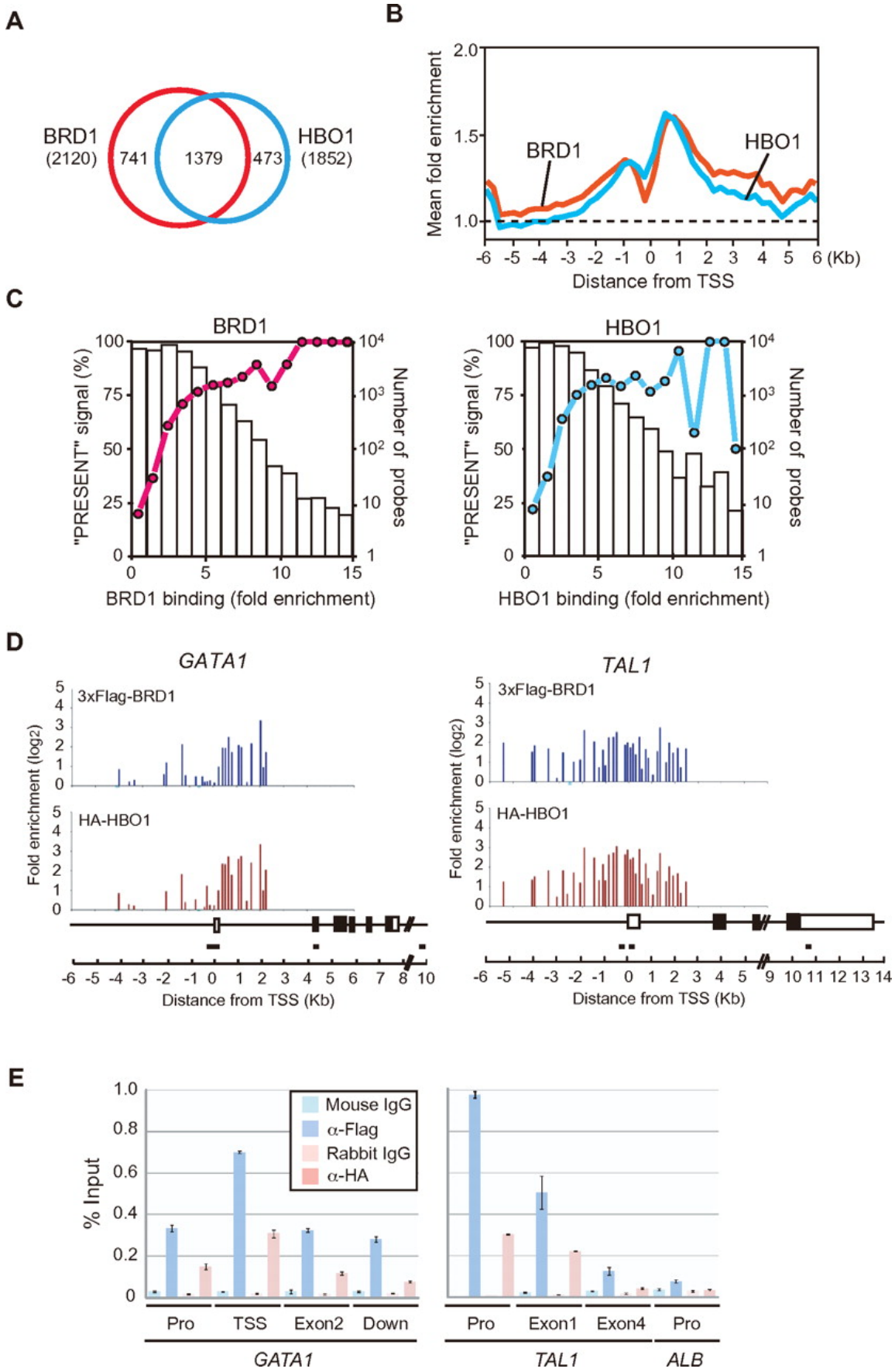

Figure 5. BRD1 and HBO1 coregulate erythroid genes.

(A) ChIP-chip analysis of BRD1 and HBO1 binding in K562 cells.A ChIP-chip

analysis was performed in K562 cells coexpressing 3xFlag-BRD1 and HA-HBO1 by use of anti-Flag and HA antibodies. Fold enrichment > 4 was judged as positive. The number of genes in each category of the Venn diagram is indicated. (B) Average BRD1 and HBO1 binding was depicted in the promoter regions (from −6 kb to +6 kb relative to the transcription start site) of all genes in the ChIP-on-chip analysis. The dotted line represents the normalized average signal over the entire chip. (C) Graph of the correlation of expressed genes in K562 cells in terms of the degree of BRD1 or HBO1 binding. Gene expression profiles of K562 cells examined with microarrays were used to judge the transcriptional status of the BRD1- or HBO1-occupied genes identified in the ChIP-chip analysis. The percentage of probes that produced "PRESENT" signals in the microarray analysis was plotted against the BRD1 or HBO1 binding detected in the ChIP-on-chip analysis. (D) ChIP-on-chip signals in the GATA1 and TAL1 promoter regions. Blue columns indicate the probes with no signals. The GATA1 and TAL1 gene structures and the location of the primer sets are depicted. (E) ChIP analyses at the GATA1 and TAL1 loci. The binding of BRD1 and HBO1 to the indicated regions of the GATA1 and TAL1 genes was determined by ChIP and site-specific real-time PCR. The relative amount of immunoprecipitated DNA is depicted as a percentage of input DNA. The data are shown as the mean ± SE for triplicate PCRs. The ALB promoter served as a negative control. Pro indicates promoter; and Down, 3 kb downstream from the polyadenylation site.

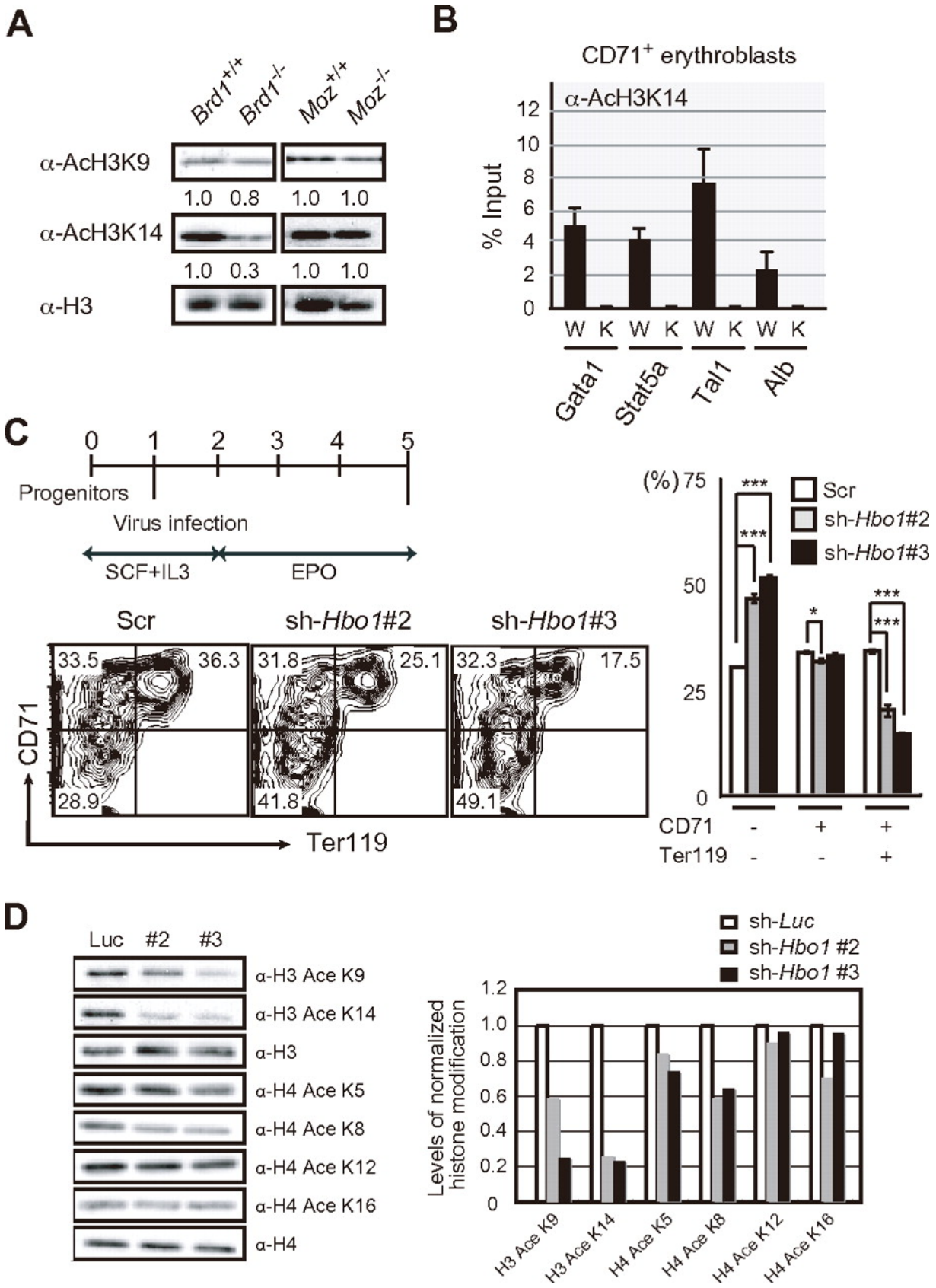

Figure 6. The Hbo1-Brd1 complex is responsible for the bulk of H3K14 acetylation.

(A) Levels of acetylation at histone H3 in wild-type, *Brd1*$^{-/-}$, and *Moz*$^{-/-}$ CD71^{+}Ter119^{-} erythroblasts. Histones purified from purified

$CD71^{+}Ter119^{-}$ erythroblasts were analyzed by Western blotting by use of the indicated antibodies. Levels of acetylated H3K9 and H3K14 were normalized to the amount of H3 and are indicated relative to wild-type control values. (B) Levels of H3K14 acetylation at the promoters of erythroid regulator genes. A ChIP analysis was performed with $CD71^{+}$ erythroblasts from wild-type (W) and *Brd1*$^{-/-}$ (K) 12.5 dpc fetal livers with an anti-acetylated H3K14 antibody. The relative amount of immunoprecipitated DNA is depicted as a percentage of input DNA. The data are shown as the mean ± SE for triplicate PCRs. The *Alb* promoter served as a negative control. (C) *Hbo1* knockdown in fetal liver progenitor cells. c-Kit^{+} $CD71^{-}$ cells were sorted from fetal livers at 12.5 dpc and cultured in the presence of SCF and IL3. Twenty-four hours later, cells were infected with lentiviruses against *Hbo1* (#2 and #3) and the culture medium was changed to that containing EPO to induce erythroid differentiation (top left). After a 3-day induction, cells were stained with the indicated antibodies and analyzed by flow cytometry. The knockdown cells were monitored for expression of GFP, a marker antigen for infection. The flow cytometric profiles of GFP^{+} cells are indicated (bottom left) and their differentiation defined by the expression of CD71 and Ter119 is shown as the mean ± SE for triplicate cultures (right). * $P < .05$, *** $P < .0005$. (D) Levels of acetylation of histones H3 and H4 in *Hbo1*-knockdown erythroblasts. Histones were prepared from $CD71^{+}$ erythroblasts purified from the *Hbo1*-knockdown culture in (C) and analyzed by Western blotting by the use of the indicated antibodies (left). Levels of acetylation of H3 and H4 at each residue were normalized to the amount of H3 and H4, respectively. The acetylation levels relative to the sh-*Luc* controls are indicated (right).

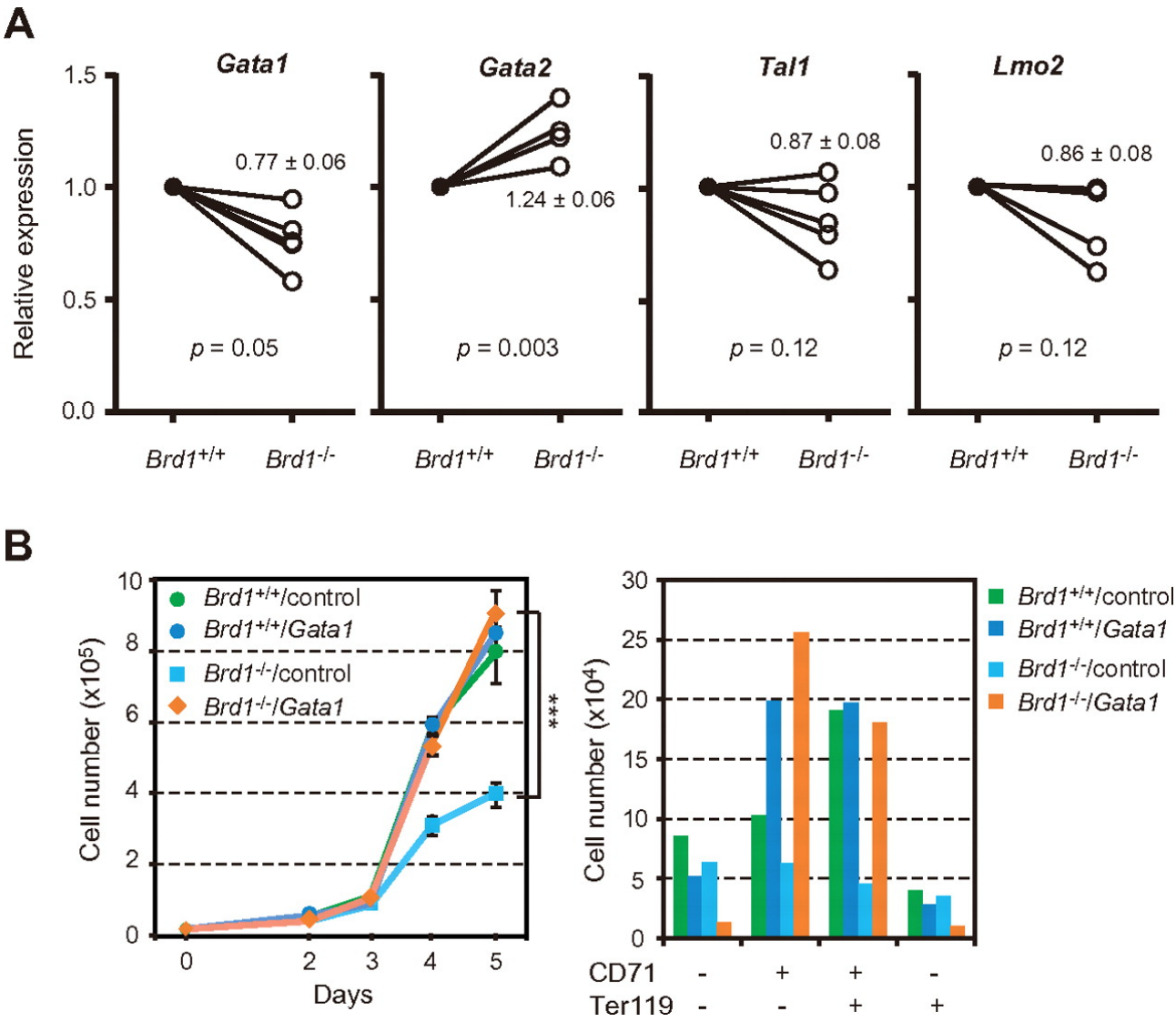

Figure 7. Insufficient transcription of erythroid regulator genes causes impaired erythropoiesis in *Brd1*$^{-/-}$ fetal livers.

(A) Quantitative RT-PCR analysis of expression of erythroid transcription factor genes in erythroblasts purified from wild-type and *Brd1*$^{-/-}$ 12.5 dpc fetal livers. mRNA levels were normalized to Hprt1 expression. Expression levels relative to those in the wild-type erythroblasts are shown as the mean ± SE (n = 4∼5). (B) Rescue of defective proliferation of *Brd1*$^{-/-}$ erythroblasts by exogenous Gata1. c-Kit^{+} CD71^{-} cells were sorted from wild-type (*Brd1*$^{+/+}$) and *Brd1*$^{-/-}$ fetal livers at 12.5 dpc and cultured in the presence of SCF and IL-3. Twenty-four hours later, cells were infected with either *GFP* control or *Gata1* retroviruses and the

culture medium was changed to that containing EPO to induce erythroid differentiation. After a 3-day induction, cells were stained with the indicated antibodies and analyzed by flow cytometry. Cell growth during culture (left) and the final numbers of erythroid cells at different stages of differentiation ($CD71^{-}Ter119^{-}$ to $CD71^{-}Te119^{+}$; right) are shown as mean ± SE for triplicate cultures. ***P < .0005.

Supplementary Figures

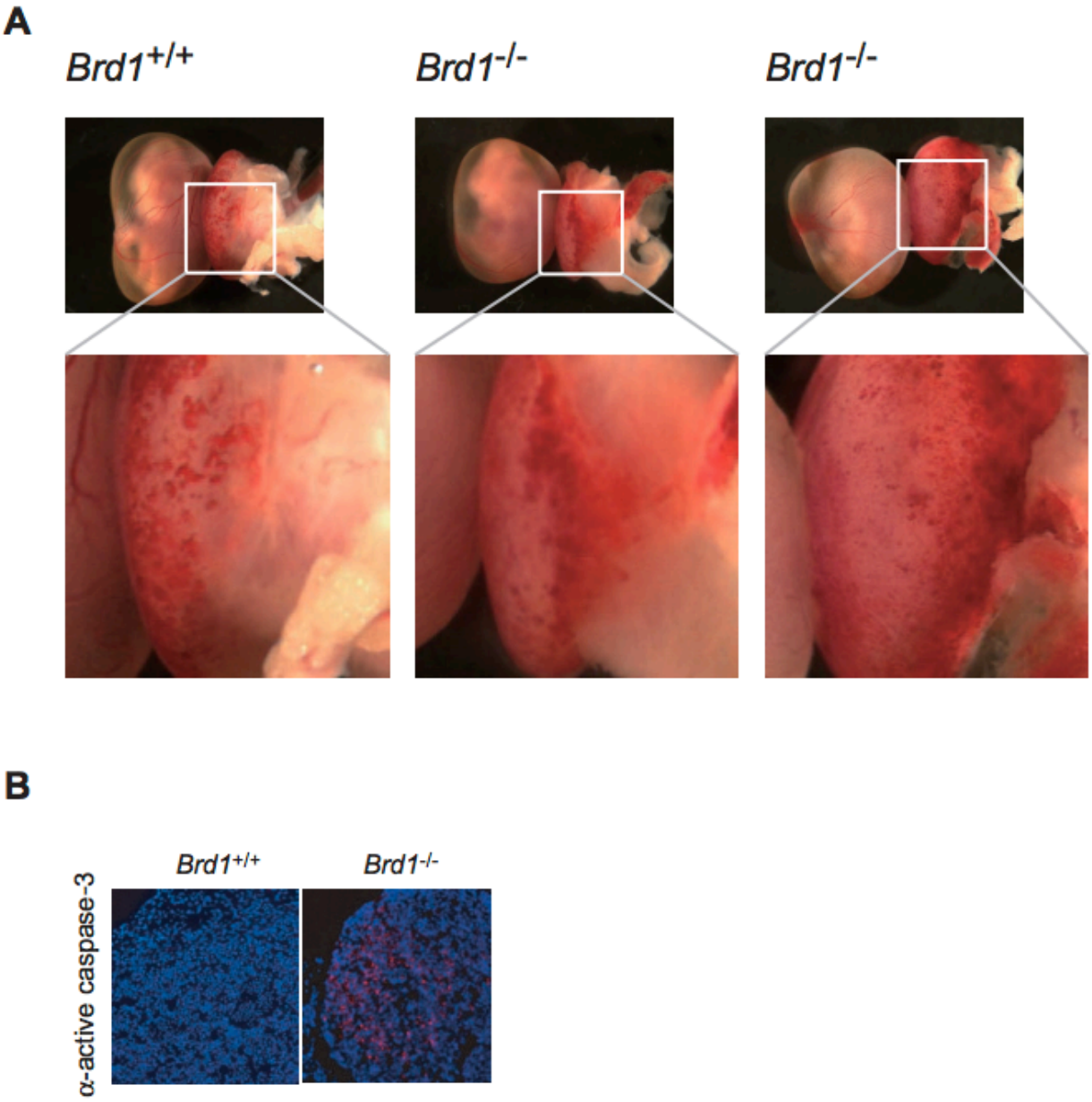

Figure S1. Yolk sac and fetal liver hematopoiesis in *Brd1*$^{-/-}$ embryos.

(A) Appearance of wild-type and *Brd1*$^{-/-}$ yolk sac at 12.5 dpc. A magnified image of the boxed area is depicted below. (B) Frozen sections of fetal livers at 12.5 dpc were stained with an anti-active caspase-3 antibody (red). Nuclear DAPI staining is in blue.

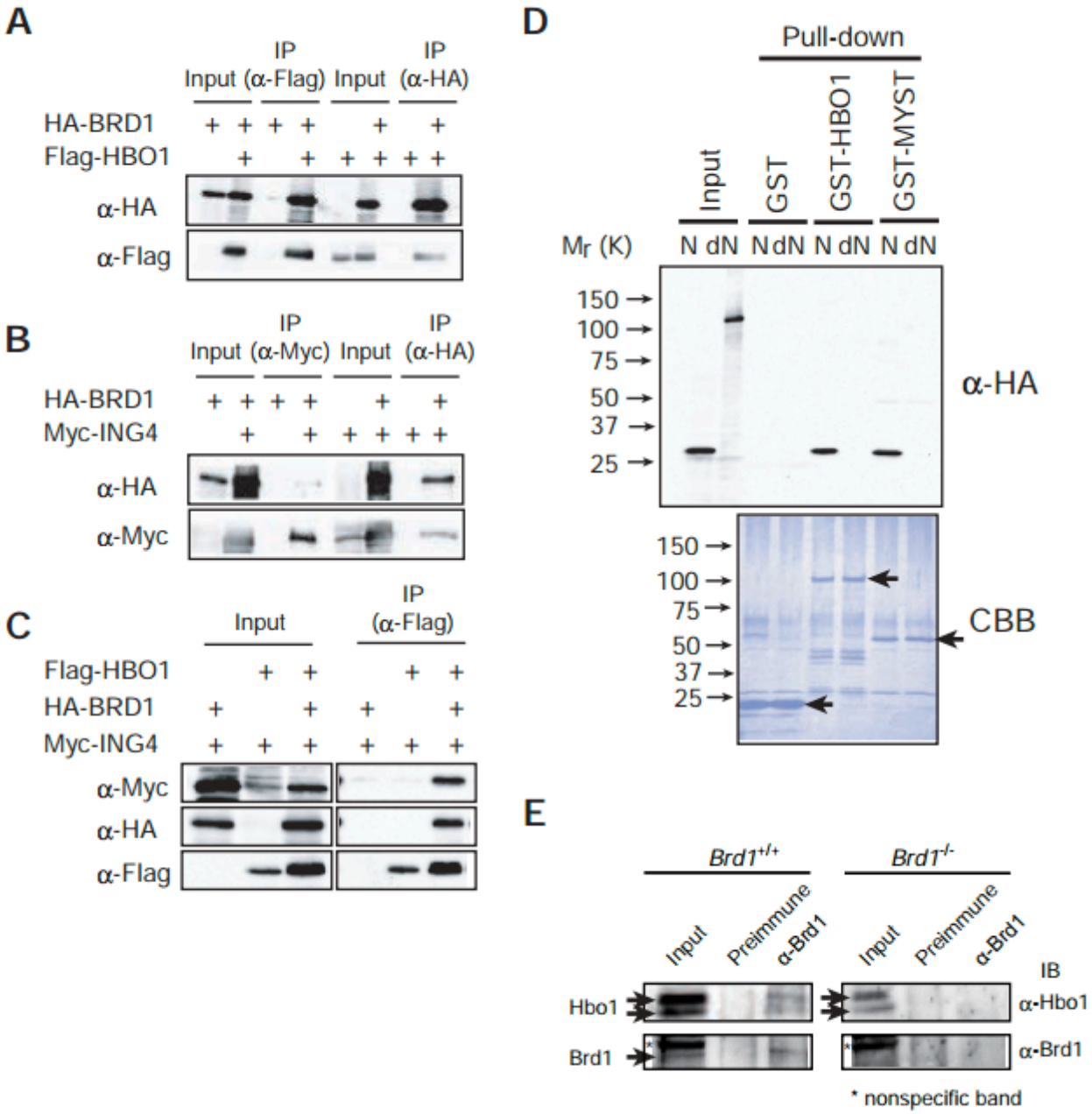

Figure S2. Physical interaction among HBO1, BRD1, and ING4 in the complex.

(A-C) Physical interaction among HBO1, BRD1, and ING4 in the complex. 293T cells were transfected with different combinations of BRD1, HBO1, and ING4 genes. Proteins in the lysates of the transfectants were immunoprecipitated with anti-FLAG, HA, or Myc antibodies. The immunoprecipitates were analyzed by Western blotting using anti-Flag, HA, or Myc antibodies. (D) GST pull-down assay. The N-terminus of BRD1 (1-198)(N) and N-terminus-deleted form of BRD1 (192-1189)(dN) were incubated with GST, full-length HBO1 fused to

GST (GST-HBO1), and the HBO1 MYST domain fused to GST (GST-MYST) in vitro. Specific binding was confirmed by Western blotting using an anti-HA antibody (upper panel). The presence of purified GST-fusion proteins was confirmed by SDS/PAGE followed by Coomassie Brilliant Blue staining (lower panel). The band corresponding to each GST-fusion protein is indicated by an arrow. (E) Interaction of endogenous Brd1 with Hbo1 in the whole embryo at 12.5 dpc. Proteins in the lysates of the whole embryos were immunoprecipitated with an anti-Brd1 antibody. The immunoprecipitates were analyzed by Western blotting using anti-Hbo1 antibody.

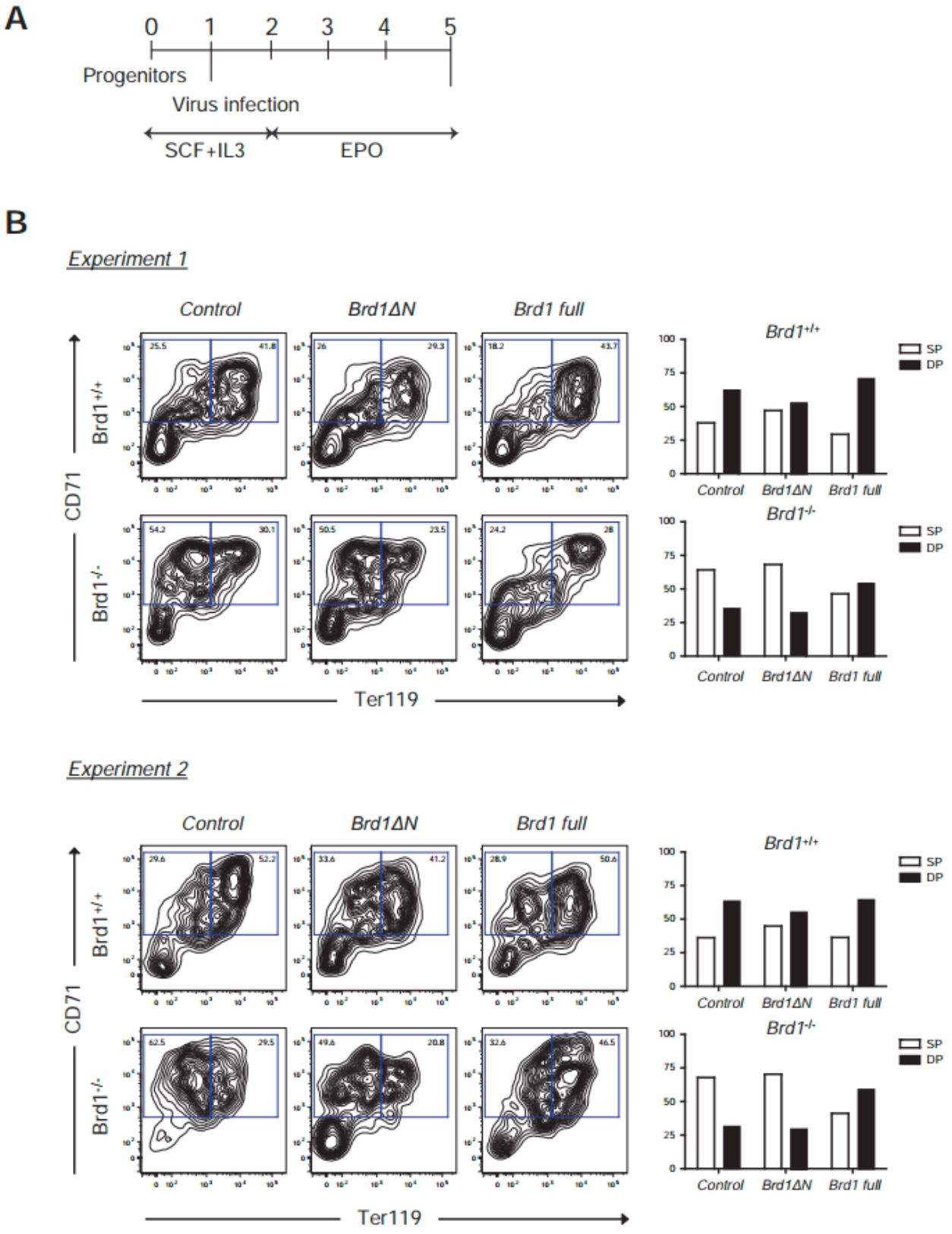

Figure S3. Rescue of defective differentiatio of *Brd1*$^{-/-}$ erythroblasts by exogenous Brd1.

(A) Experimental design. c-Kit^{+} CD71^{-} progenitors were sorted from wild-type

and Brd1$^{-/-}$ fetal livers at 12.5 dpc and cultured in the presence of SCF and IL3. Twenty-four hours later, cells were infected with *GFP* control, full-length *Brd1*, or *Brd1*ΔN retroviruses and the culture medium was changed to that containing EPO to induce erythroid differentiation. After a 3-day induction, cells were stained with anti-CD71 and Ter119 antibodies and analyzed by flow cytometry. (B) Flow cytometric profiles of cells infected with the indicated retroviruses is depicted in the left panels. The proportion of cells in the CD71^{+}Ter119^{-} (single positive, SP) and CD71^{+}Te119^{+} (double positive, DP) fractions among the total CD71^{+} cells (CD71^{+}Ter119^{-} and CD71^{+}Te119^{+}) were indicated in the right panels. Two independent experiments were performed.

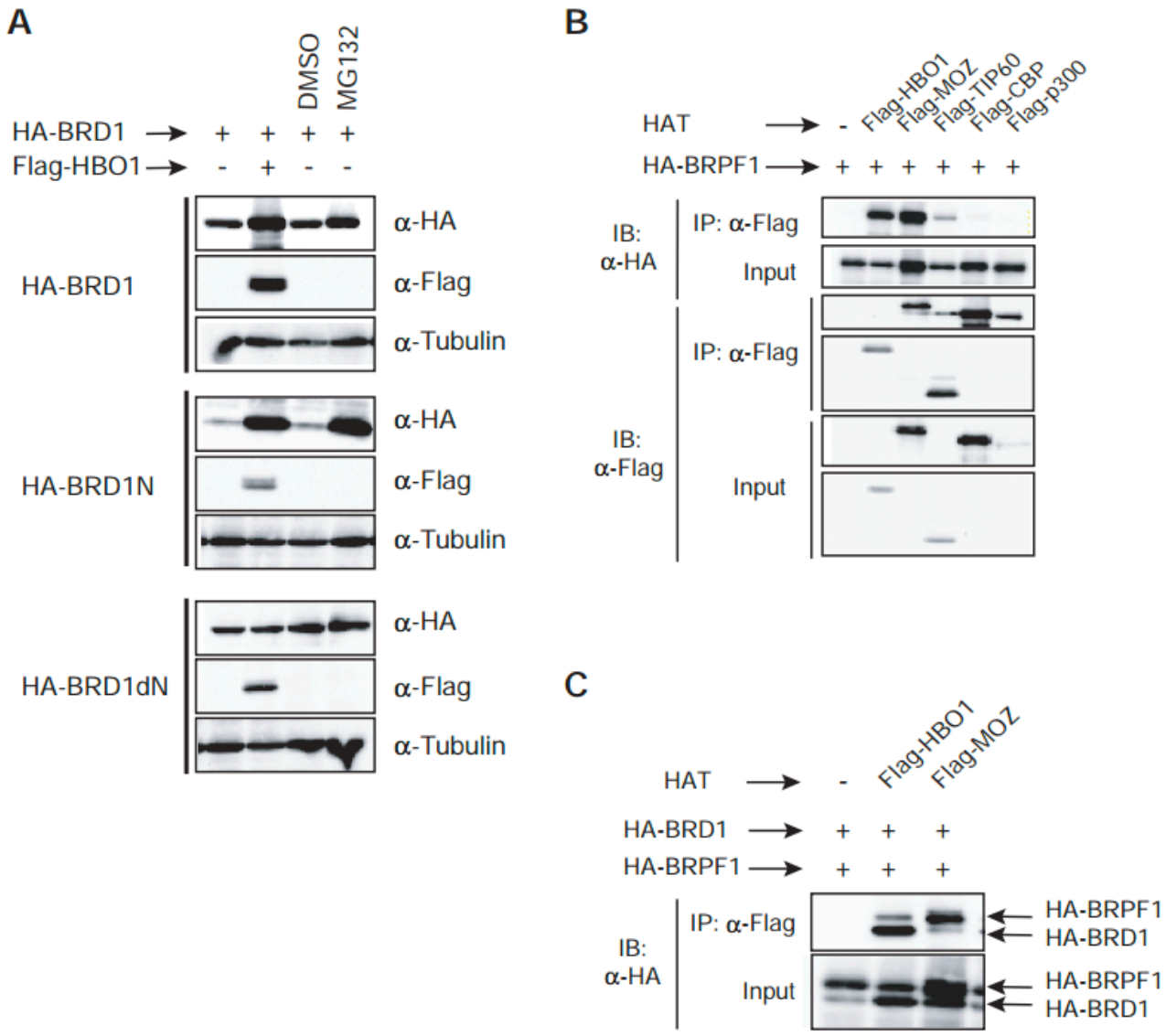

Figure S4. Stability of the BRD1 protein and the affinity of BRD1 for the MYST family HATs.

(A) 293T cells were transfected with an HA-tagged full-length BRD1 (HA-Brd1), the N-terminus of Brd1 (1-198, HA-Brd1N) and an N-terminus-deleted form of Brd1 (192-1189, HA-Brd1dN) with and without Flag-tagged HBO1. The cells were treated with MG132 (20 μm) or DMSO (control) for 4 hours. Brd1 was detected by Western blotting using an anti-HA antibody. The level of α-Tubulin is shown as a control. (B) Affinity of BRPF1 for the MYST family HATs (HBO1, MOZ, and Tip60) and CBP/p300. 293T cells were transfected with HA-tagged BRPF1 together with indicated Flag-tagged HATs. Proteins in the lysates of the

transfectants were immunoprecipitated with an anti-FLAG antibody. The immunoprecipitates were analyzed by Western blotting using anti-Flag and HA antibodies. (C) Competitive binding assay of BRD1 and BRPF1 to HBO1 and MOZ. 293T cells were transfected with HA-tagged BRD1 and BRPF1 together with Flag-tagged HBO1 or MOZ. Proteins in the lysates of the transfectants were immunoprecipitated with the anti-FLAG antibody. The immunoprecipitates were analyzed by Western blotting using an anti-HA antibody.

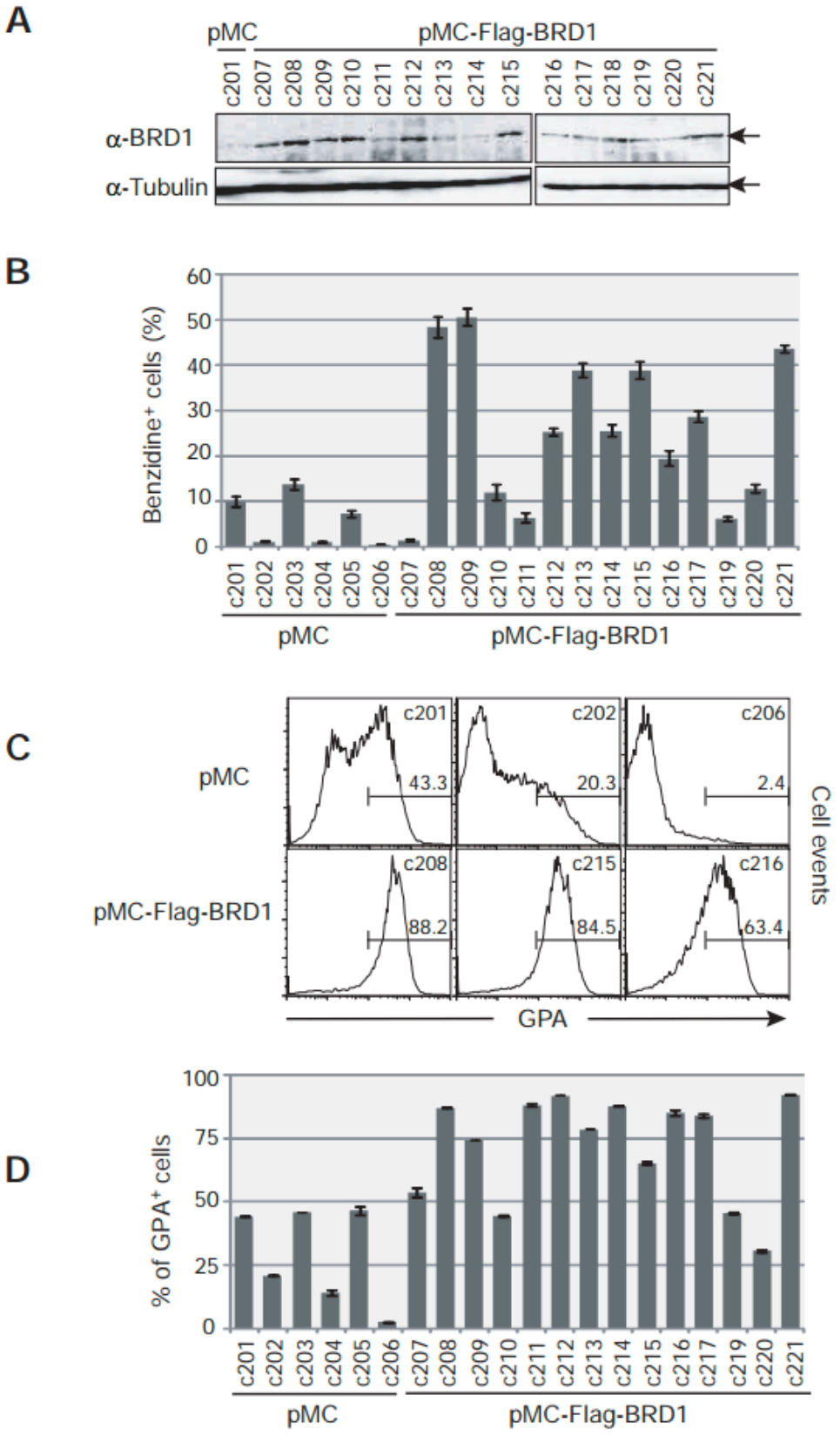
A
pMC
pMC-Flag-BRD1
c201 c207 c208 c209 c210 c211 c212 c213 c214 c215 c216 c217 c218 c219 c220 c221
α-BRD1
α-Tubulin
B
Benzidine+ cells (%)
60
50
40
30
20
10
0
c201 c202 c203 c204 c205 c206 c207 c208 c209 c210 c211 c212 c213 c214 c215 c216 c217 c219 c220 c221
pMC
pMC-Flag-BRD1
C
pMC
pMC-Flag-BRD1
c201
43.3
c202
20.3
c206
2.4
c208
88.2
c215
84.5
c216
63.4
Cell events
GPA
D
% of GPA+ cells
100
75
50
25
0
c201 c202 c203 c204 c205 c206 c207 c208 c209 c210 c211 c212 c213 c214 c215 c216 c217 c219 c220 c221
pMC
pMC-Flag-BRD1

Figure S5. Effect of enforced expression of BRD1 on erythroid differentiation of K562 cells.

(A) Expression of BRD1 in K562 cells transduced with an empty retrovirus vector (pMC) or retroviruses expressing Flag-BRD1. BRD1 expression was detected by Western blotting using an anti-FLAG antibody. The level of α-Tubulin is shown as a control. (B) Benzidine staining of K562 clones. The data is shown as the mean ± S.E. (C) Representative flow cytometric profiles of GPA expression in K562 clones. Percentages of GPA-positive cells are indicated. (D) The percentage of GPA-positive cells of each K562 clone is shown as the mean ± S.E.

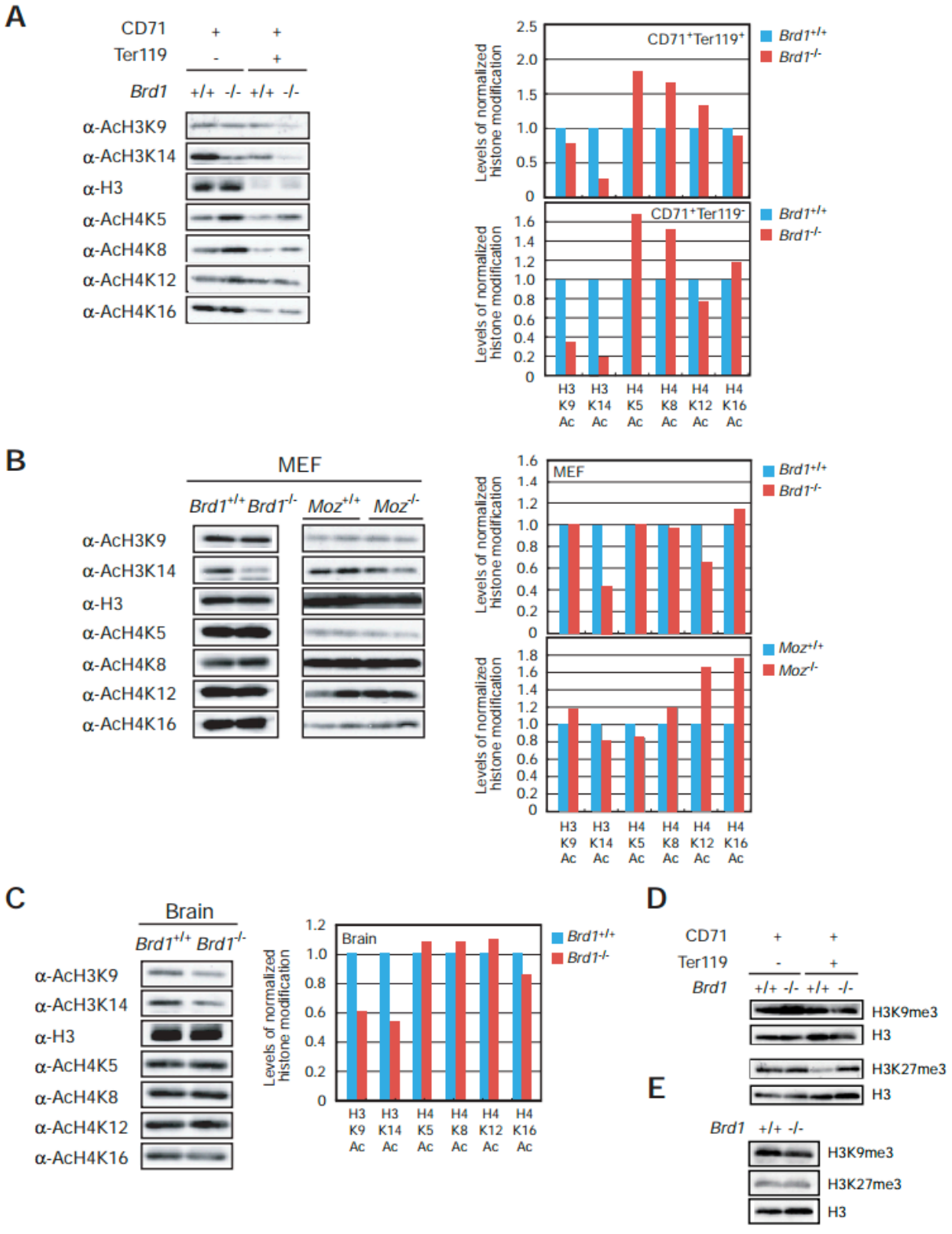

Figure S6. Levels of acetylation at H3 and H4 in *Brd1*$^{-/-}$ erythroblasts, MEFs, and brain.

Levels of acetylation at H3 and H4 in *Brd1*$^{-/-}$ and *Moz*$^{-/-}$ erythroblasts (A) and

MEFs (B), and Brd1$^{-/-}$ brain (C). Histones were extracted from fetal liver erythroblasts (CD71^{+}Ter119^{-} and CD71^{+}Ter119^{+}), brain at 12.5 dpc, and MEFs prepared from embryos at 12.5 dpc and then analyzed by Western blotting using the indicated antibodies (left panels). Levels of acetylation at each histone residue were normalized to the amount of H3 and are indicated relative to the control values (right panels). (D, E) Levels of trimethylation at H3K9 and H3K27 in *Brd1*$^{-/-}$ erythroblasts (D) and MEFs (E). Histones were prepared as in A and B.

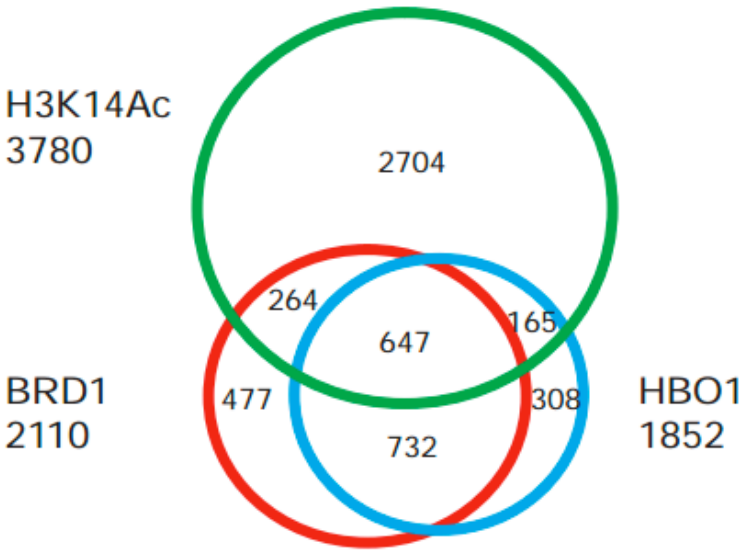

Figure S7. Relationship between acetylation at H3K14 and BRD1-HBO1 binding.

ChIP-chip analyses was performed in K562 cells co-expressing 3xFlag-BRD1 and HA-HBO1 using an anti-acetylated H3K14 antibody. Fold enrichment greater than 2 was judged as positive. The data was compared with those obtained in Figure 5A. The number of genes in each category of the Venn diagram is indicated.

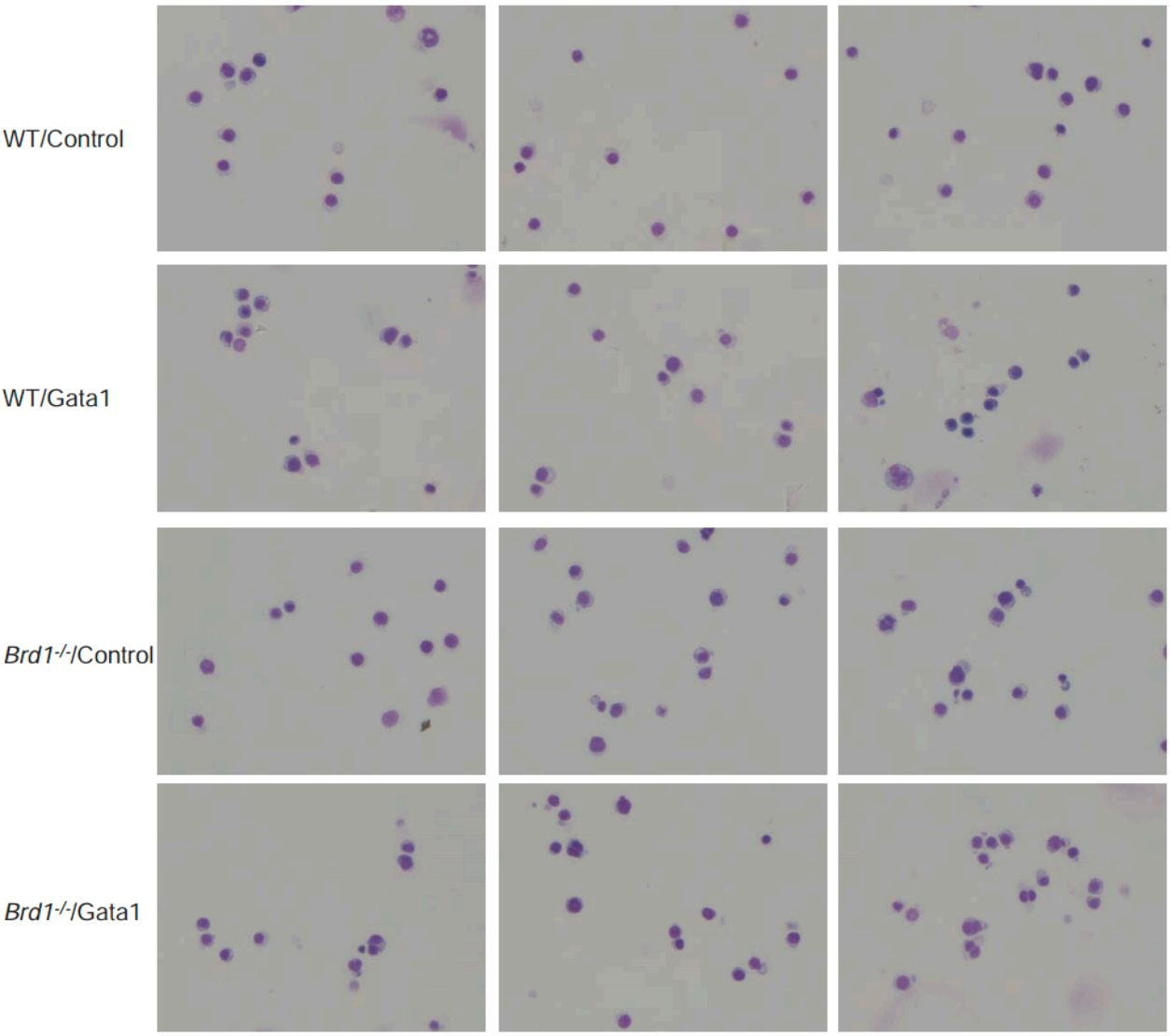

Figure S8. Morphology of *Brd1*$^{-/-}$ CD71^{+}Ter119^{+} erythroblasts.

c-Kit^{+}CD71^{-} cells were sorted from wild-type (WT) and Brd1$^{-/-}$ fetal livers at 12.5 dpc and cultured in the presence of SCF and IL-3. Twenty-four hours later, cells were infected with either GFP control or Gata1 retroviruses and the culture medium was changed to that containing EPO to induce erythroid differentiation. After a 3-day induction, CD71^{+}Ter119^{+} erythroblasts were purified by cell sorting, cytospun onto slide glasses, and then subjected to morphological analysis by May-Gruenwald-Giemsa staining.

Acknowledgements

I would like to express my grateful thanks to Professor Naoto Yamaguchi, Department of Molecular Cell Biology, Graduate School of Pharmaceutical Sciences, Chiba University, Professor Atsushi Iwama, and Assistant Professor Satoru Miyagi, Department of Cellular and Molecular Medicine, Graduate School of Medicine, Chiba University for their invaluable guidance, suggestions, supervision, kindness and continuous encouragement.

I am indebted to Drs Masayoshi Iizuka and Matthias Hammerschmidt for providing the pFLAG-HBO1 and pcDNA3-Flag-Brpf1 vectors, respectively; Atsunori Saraya and Makiko Yui for their technical assistance; and Drs Kiyotaka Toshimori and Tohru Mutoh for technical advice on the histochemical analyses.

References

1. Avvakumov N, Côté J. The myst family of histone acetyltransferases and their intimate links to cancer. *Oncogene*. 2007;26(37):5395–407.

2. Lee KK, Workman JL. Histone acetyltransferase complexes: one size doesn't fit all. *Nature reviews. Molecular cell biology*. 2007;8(4):284–95.

3. Doyon Y, Cayrou C, Ullah M, et al. Ing tumor suppressor proteins are critical regulators of chromatin acetylation required for genome expression and perpetuation. *Molecular cell*. 2006;21(1):51–64.

4. Ullah M, Pelletier N, Xiao L, et al. Molecular architecture of quartet moz/morf histone acetyltransferase complexes. *Molecular and cellular biology*. 2008;28(22):6828–43.

5. Hung T, Binda O, Champagne KS, et al. Ing4 mediates crosstalk between histone h3 k4 trimethylation and h3 acetylation to attenuate cellular transformation. *Molecular cell*. 2009;33(2):248–56.

6. Saksouk N, Avvakumov N, Champagne KS, et al. Hbo1 hat complexes target chromatin throughout gene coding regions via multiple phd finger interactions with histone h3 tail. *Molecular cell*. 2009;33(2):257–65.

7. Taverna SD, Ilin S, Rogers RS, et al. Yng1 phd finger binding to h3 trimethylated at k4 promotes nua3 hat activity at k14 of h3 and transcription at a subset of targeted orfs. *Molecular cell*. 2006;24(5):785–96.

8. Katsumoto T, Aikawa Y, Iwama A, et al. Moz is essential for maintenance of hematopoietic stem cells. *Genes & development*. 2006;20(10):1321–30.

9. Thomas T, Corcoran LM, Gugasyan R, et al. Monocytic leukemia zinc finger protein is essential for the development of long-term reconstituting hematopoietic stem cells. *Genes & development*. 2006;20(9):1175–86.

10. Crump JG, Swartz ME, Eberhart JK, Kimmel CB. Moz-dependent hox expression controls segment-specific fate maps of skeletal precursors in the face. *Development (Cambridge, England)*. 2006;133(14):2661–9.

11. Laue K, Daujat S, Crump JG, et al. The multidomain protein brpf1 binds histones and is required for hox gene expression and segmental identity. *Development (Cambridge, England)*. 2008;135(11):1935–46.

12. Hibiya K, Katsumoto T, Kondo T, Kitabayashi I, Kudo A. Brpf1, a subunit of the moz histone acetyl transferase complex, maintains expression of anterior and posterior hox genes for proper patterning of craniofacial and caudal skeletons. *Developmental biology*. 2009;329(2):176–90.

13. McCullagh P, Chaplin T, Meerabux J, et al. The cloning, mapping and expression of a novel gene, brl, related to the af10 leukaemia gene. *Oncogene*. 1999;18(52):7442–52.

14. Kitamura T, Koshino Y, Shibata F, et al. Retrovirus-mediated gene transfer and expression cloning: powerful tools in functional genomics. *Experimental hematology*. 2003;31(11):1007–14.

15. Iwama A, Oguro H, Negishi M, et al. Enhanced self-renewal of hematopoietic stem cells mediated by the polycomb gene product bmi-1. *Immunity*. 2004;21(6):843–51.

16. Katayama K, Wada K, Miyoshi H, et al. Rna interfering approach for clarifying the ppargamma pathway using lentiviral vector expressing short hairpin rna. *FEBS letters*. 2004;560(1-3):178–82.

17. Kitabayashi I, Aikawa Y, Nguyen LA, Yokoyama A, Ohki M. Activation of aml1-mediated transcription by moz and inhibition by the moz-cbp fusion protein. *The EMBO journal*. 2001;20(24):7184–96.

18. Kimura H, Hayashi-Takanaka Y, Goto Y, Takizawa N, Nozaki N. The organization of histone h3 modifications as revealed by a panel of specific monoclonal antibodies. *Cell structure and function*. 2008;33(1):61–73.

19. Endoh M, Endo TA, Endoh T, et al. Polycomb group proteins ring1a/b are functionally linked to the core transcriptional regulatory circuitry to maintain es cell identity. *Development (Cambridge, England)*. 2008;135(8):1513–24.

20. Foy RL, Song IY, Chitalia VC, et al. Role of jade-1 in the histone acetyltransferase (hat) hbo1 complex. *The Journal of biological chemistry*. 2008;283(43):28817–26.

21. Addya S, Keller MA, Delgrosso K, et al. Erythroid-induced commitment of k562 cells results in clusters of differentially expressed genes enriched for specific transcription regulatory elements. *Physiological genomics*. 2004;19(1):117–30.

22. Pevny L, Simon MC, Robertson E, et al. Erythroid differentiation in chimaeric mice blocked by a targeted mutation in the gene for transcription factor gata-1. *Nature*. 1991;349(6306):257–60.

23. Weiss MJ, Orkin SH. Transcription factor gata-1 permits survival and maturation of erythroid precursors by preventing apoptosis. *Proceedings of the National Academy of Sciences of the United States of America*. 1995;92(21):9623–7.

24. Cantor AB, Orkin SH. Transcriptional regulation of erythropoiesis: an affair involving multiple partners. *Oncogene*. 2002;21(21):3368–76.

25. Mikkola HKA, Klintman J, Yang H, et al. Haematopoietic stem cells retain long-term repopulating activity and multipotency in the absence of stem-cell leukaemia scl/tal-1 gene. *Nature*. 2003;421(6922):547–51.

26. Kaneko H, Shimizu R, Yamamoto M. Gata factor switching during erythroid differentiation. *Current opinion in hematology*. 2010;17(3):163–8.

27. Grass JA, Boyer ME, Pal S, et al. Gata-1-dependent transcriptional repression of gata-2 via disruption of positive autoregulation and domain-wide chromatin remodeling. *Proceedings of the National Academy of Sciences of the United States of America*. 2003;100(15):8811–6.

28. Fujiwara T, O'Geen H, Keles S, et al. Discovering hematopoietic mechanisms through genome-wide analysis of gata factor chromatin occupancy. *Molecular cell*. 2009;36(4):667–81.

29. Kueh AJ, Dixon MP, Voss AK, Thomas T. Hbo1 is required for h3k14 acetylation and normal transcriptional activity during embryonic development. *Molecular and cellular biology*. 2011;31(4):845–60.

30. Voss AK, Collin C, Dixon MP, Thomas T. Moz and retinoic acid coordinately regulate h3k9 acetylation, hox gene expression, and segment identity. *Developmental cell*. 2009;17(5):674–86.

31. Iizuka M, Stillman B. Histone acetyltransferase hbo1 interacts with the orc1 subunit of the human initiator protein. *The Journal of biological chemistry*. 1999;274(33):23027–34.

32. Burke TW, Cook JG, Asano M, Nevins JR. Replication factors mcm2 and orc1 interact with the histone acetyltransferase hbo1. *The Journal of biological chemistry*. 2001;276(18):15397–408.

33. Iizuka M, Matsui T, Takisawa H, Smith MM. Regulation of replication licensing by acetyltransferase hbo1. *Molecular and cellular biology*. 2006;26(3):1098–108.

34. Miotto B, Struhl K. Hbo1 histone acetylase is a coactivator of the replication licensing factor cdt1. *Genes & development*. 2008;22(19):2633–8.

35. Agalioti T, Chen G, Thanos D. Deciphering the transcriptional histone acetylation code for a human gene. *Cell*. 2002;111(3):381–92.

36. Vicent GP, Zaurin R, Nacht AS, et al. Two chromatin remodeling activities cooperate during activation of hormone responsive promoters. *PLoS genetics*. 2009;5(7):e1000567.

37. Vezzoli A, Bonadies N, Allen MD, et al. Molecular basis of histone h3k36me3 recognition by the pwwp domain of brpf1. *Nature structural & molecular biology*. 2010;17(5):617–9.

38. Iizuka M, Takahashi Y, Mizzen CA, et al. Histone acetyltransferase hbo1: catalytic activity, cellular abundance, and links to primary cancers. *Gene*. 2009;436(1-2):108–14.

39. Nebral K, Denk D, Attarbaschi A, et al. Incidence and diversity of pax5 fusion genes in childhood acute lymphoblastic leukemia. *Leukemia : official journal of the Leukemia Society of America, Leukemia Research Fund, U.K.* 2009;23(1):134–43.

List of Publications

[Main Thesis Publication]

Yuta Mishima, Satoru Miyagi, Atsunori Saraya, Masamitsu Negishi, Mitsuhiro Endoh, Takaho A Endo, Tetsuro Toyoda, Jun Shinga, Takuo Katsumoto, Tetsuhiro Chiba, Naoto Yamaguchi, Issay Kitabayashi, Haruhiko Koseki, and Atsushi Iwama

The Hbo1-Brd1/Brpf2 complex is responsible for global acetylation of H3K14 and required for fetal liver erythropoiesis. *Blood*. 1; 118(9): 2443-2453, 2011.

[Reference Publication]

Makiko Mochizuki-Kashio, Yuta Mishima, Satoru Miyagi, Masamitsu Negishi, Atsunori Saraya, Takaaki Konuma, Jun Shinga, Haruhiko Koseki, and Atsushi Iwama

Dependency on the polycomb gene Ezh2 distinguishes fetal from adult hematopoietic stem cells. *Blood*. 15; 118(25): 6553-6561, 2011.

This thesis for the doctorate in Pharmaceutical Sciences was examined by the following referees authorized by the Graduate School of Pharmaceutical Science, Chiba University

Examiners

Dr. Toshihiko Murayama, Ph.D. Professor of Chiba University

(Graduate School of Pharmaceutical Sciences) *Chief examiner*

Dr. Motoyuki Itoh, Ph.D. Professor of Chiba University

(Graduate School of Pharmaceutical Sciences)

Dr. Masahiko Hatano, M.D., Ph.D. Professor of Chiba University

(Graduate School of Medicine)